INTERNATIONAL JOURNAL FOR NUMERICAL METHODS IN FLUIDS
Int. J. Numer. Meth. Fluids 2004; **45**:839–887 (DOI: 10.1002/fld.719)

Generalized Fourier analyses of the advection–diffusion equation—Part I: one-dimensional domains

Mark A. Christon, Mario J. Martinez and Thomas E. Voth*,†

Sandia National Laboratories, M/S 0819, P.O. Box 5800, Albuquerque 87185-0819, New Mexico

SUMMARY

This paper presents a detailed multi-methods comparison of the spatial errors associated with finite difference, finite element and finite volume semi-discretizations of the scalar advection–diffusion equation. The errors are reported in terms of non-dimensional phase and group speed, discrete diffusivity, artificial diffusivity, and grid-induced anisotropy. It is demonstrated that Fourier analysis provides an automatic process for separating the discrete advective operator into its symmetric and skew-symmetric components and characterizing the spectral behaviour of each operator. For each of the numerical methods considered, asymptotic truncation error and resolution estimates are presented for the limiting cases of pure advection and pure diffusion. It is demonstrated that streamline upwind Petrov–Galerkin and its control-volume finite element analogue, the streamline upwind control-volume method, produce both an artificial diffusivity and a concomitant phase speed adjustment in addition to the usual semi-discrete artifacts observed in the phase speed, group speed and diffusivity. The Galerkin finite element method and its streamline upwind derivatives are shown to exhibit super-convergent behaviour in terms of phase and group speed when a consistent mass matrix is used in the formulation. In contrast, the CVFEM method and its streamline upwind derivatives yield strictly second-order behaviour. In Part II of this paper, we consider two-dimensional semi-discretizations of the advection–diffusion equation and also assess the affects of grid-induced anisotropy observed in the non-dimensional phase speed, and the discrete and artificial diffusivities. Although this work can only be considered a first step in a comprehensive multi-methods analysis and comparison, it serves to identify some of the relative strengths and weaknesses of multiple numerical methods in a common analysis framework. Published in 2004 by John Wiley & Sons, Ltd.

KEY WORDS: advection–diffusion; phase error; dispersion; discrete diffusivity; artificial viscosity

1. INTRODUCTION

Numerical methods for the solution of partial differential equations have evolved to the point where the ‘end-user’ is faced with choosing from a plethora of formulations, e.g. finite difference, finite volume or finite element, upwind or stabilization techniques, structured or unstruc-

*Correspondence to: T. E. Voth, Computational Physics R&D Department, Sandia National Laboratories, M/S 0819, P.O. Box 5800, Albuquerque 87185-0819, New Mexico.
†E-mail: tevoth@sandia.gov

Published online 4 May 2004
Received 17 April 2003
Revised 11 February 2004

tured grids, mesh-full or mesh-free, etc. Each choice has its individual strengths and weaknesses. In order to understand the differences and similarities between competing methods, an initiative to perform a multi-methods comparison based on numerical and computational performance has been launched.

The comparison of numerical methods can be based on a number of metrics such as truncation error, rate of convergence, and dispersive and diffusive behaviour. Such a comparison between dissimilar methods is difficult because it may not be possible to select criteria that 'fairly' represent each method. For example, the best way to compare finite difference methods that are based on Taylor series with finite element methods that may be best represented by errors measured in the energy norm is an open question.

As a first step in this multi-methods analysis and comparison, we chose to apply Fourier analysis because it provides a general methodology that is capable of analysing multiple methods in a single mathematical framework while providing a great deal of information and insight into each method. In this work, we use Fourier analysis to probe the following aspects of each method: (a) numerical dispersion, i.e. phase and group velocity errors, (b) apparent, i.e. discrete, diffusivities that are wavelength dependent—spatial discretization introduces this often-ignored error, even though many schemes exhibit under-diffusive behaviour at short-wavelengths, (c) the limiting behaviour of short wavelength information for both wave propagation and diffusion, (d) the identification and characterization of artificial diffusivity introduced via upwinding, (e) grid bias errors in phase, group, discrete diffusivity and artificial diffusivity, and (f) asymptotic convergence properties and resolution requirements.

Fourier analysis provides the ability to identify and characterize the artificial diffusivity of upwind methods because, in effect, it automatically segregates the discrete advection operators into dissipative symmetric and non-dissipative skew-symmetric parts. In addition, this technique also provides insight into the asymptotic convergence of the methods without the ambiguities associated with the choice of a single error norm for multiple methods.

For this effort, a variety of finite difference, finite volume and finite element methods are considered. Each method is considered on both one- and two-dimensional periodic Cartesian grids. Attention has been restricted to the following advective schemes: first through third-order upwind and second-order centered differences, QUICK, and Fromm's method. Here, Fromm's method is considered in a semi-discrete form, i.e. in the limit as $\Delta t \rightarrow 0$, for the purposes of analysis rather than in its original fractional-step form [1]. For the finite element methods both Galerkin (FEM) and streamline-upwind Petrov–Galerkin (FEM-SUPG) formulations are considered. The finite volume methods include the control-volume finite element method (CVFEM) with and without the stream-line upwind analogue of SUPG known as SUCV (CVFEM-SUCV) [2, 3]. In addition, two finite volume schemes derived using least-squares gradient reconstruction (LSR) are considered.

1.1. Background and historical perspective

In general, the application of discrete solution methods to hyperbolic partial differential equations, e.g. pure advection, can result in solutions that are dispersive even though the physical model for wave propagation is non-dispersive. Dispersion errors are typically characterized by the differences between the apparent, i.e. numerical, phase and group speed of waves and their exact counterparts.

In the context of pure (linear) advection, the phase speed is the speed at which individual waves propagate. In the discrete sense, the phase speed is a function of the wavelength of the propagating wave. Therefore, phase error may be viewed as a measure of the influence of numerical dispersion on the apparent phase speed relative to the true phase speed.

In contrast to the phase speed, the group speed describes the propagation of wave packets that are comprised of short wavelength signals modulated by a slowly varying, longer wavelength envelope. Because the energy associated with a wave packet travels with the packet, the group speed is often referred to as the 'energy' velocity. The group speed is also referred to as the speed of modulation. For a non-dispersive medium the phase and group speed are identical.

In discrete advection, the group speed may be used to study and explain the propagation of short wavelength signals that are typically close to $2\Delta x$ in wavelength where Δx is the characteristic mesh spacing. Vichnevetsky [4–6] has demonstrated that spurious $2\Delta x$ oscillations, that are induced by rapid changes in mesh resolution and at physical boundaries, propagate at a group speed associated with a $2\Delta x$ wavelength.

Phase and group speed errors represent some of the most constraining numerical errors associated with the simulation of advection dominated processes (see also Reference [7]). The accurate simulation of advection dominated processes using discrete numerical schemes hinges upon having a clear understanding of the constraining numerical errors, and sufficient computational resources to effect solutions at the requisite grid scale. Examples of this may be seen when attempting to compute turbulent flow fields via direct numerical simulation (DNS) or large eddy simulation (LES). Controlling the dispersive errors, e.g. phase speed error, to within 5% for a first-order hyperbolic equation requires approximately 11–12 cells per wavelength when using traditional finite difference or lumped-mass finite element methods (see Table 2.6.2 in Reference [8]). Thus, the simulation of advection dominated problems is limited by the wavelength that the grid can accurately represent. A failure to respect the so-called grid Nyquist limit can introduce deleterious aliasing effects that corrupt the simulation fidelity.

In contrast to the phase and group errors, the application of a discrete method to the diffusive part of the advection–diffusion equation yields a discrete diffusivity that is not equivalent to the prescribed diffusivity in the partial differential equation. The discrete diffusivity exhibits wavelength dependent behaviour, and in multiple dimensions is directionally dependent. The fact that signals diffuse at different rates based on wavelength is frequently overlooked, but explains why some methods may appear to be under-diffusive in certain circumstances. We have found little discussion in the literature regarding the wavelength-dependent behaviour of the discrete diffusivity. However, the work by Jansen *et al.* [9], has dealt with improving the accuracy of low-order stabilized finite elements by including a reconstructed residual-based diffusion operator. Unfortunately, we have not yet analysed this variant of Galerkin/least-squares formulation to assess its spectral behaviour.

The use of a generalized Fourier analysis to assess dispersive and diffusive errors is not new and has been used by numerous researchers to characterize the performance of numerical methods. The effects of consistent, lumped and higher-order mass matrices on the phase speed for linear and quadratic finite elements were investigated by Belytschko and Mullen [10] for wave propagation in a linear elastic medium in one dimension. Here, it was verified that the period elongation errors associated with a trapezoidal rule time integrator can

be nearly matched with the leading phase errors introduced by a consistent mass matrix. Similarly, the period shortening associated with central differences in time can be matched with the lagging phase errors associated with mass lumping for linear elements. This compensatory interaction between the time integrator and mass matrix yielded the class of methods typically referred to as 'matched' methods found in many explicit solid dynamics codes today.

Vichnevetsky *et al.* [11, 12, 6] have investigated the dispersive nature of both finite difference and finite element methods for the first-order wave equation. In Reference [13], the dispersive errors introduced by nonuniform grid spacing and 'hard' boundaries are discussed, and the possibility of using artificial viscosity to damp these short wavelength spurious waves is investigated. Similar analysis techniques have been applied to wave propagation in periodic domains [14]. Trefethen [15] has considered the role of group velocity in understanding the propagation of wave packets, the generation of parasitic waves at interfaces, and stability. Here, the influence of group velocity in two-dimensional finite difference discretizations with uniform aspect ratio was considered. Karni [16] has characterized the group speed errors associated with symmetric upwind schemes for pure advection, i.e. a first-order wave equation.

Fourier analysis has also been applied to finite element discretizations in order to understand the dispersive nature of elastic wave propagation in bars and locking phenomena in beams [17]. This analysis technique was applied by Park and Flaggs [18] in an effort to understand and ameliorate locking phenomena in C^o plate elements. Alvin and Park [19] have also used Fourier analysis to tailor the frequency response of beams and bars discretized with the finite element method.

More recently, Shakib and Hughes [20] have applied Fourier analysis to the space–time Galerkin/least-squares (GLS) method for advection–diffusion problems. Harari and Hughes [21] present the phase error associated with the GLS discretization for the second-order wave equation in a finite domain. Deville and Mund [22] have used Fourier analysis to investigate the spectral behaviour of the iteration matrix for finite element preconditioning. Thompson and Pinsky [23] extended the concepts of Fourier analysis in order to treat p-version finite element discretizations. This work provides practical guidelines for the number of elements per wavelength in terms of the spectral order. Similarly, Grosh and Pinsky [24] have applied Fourier dispersion analysis to fluid loaded plates for structural acoustics simulations. Nance *et al.* [25] have used Fourier analysis to develop low-dispersion finite volume aeroacoustic solvers where the dispersion and dissipation are critical to the code performance. Christon [26] considered the influence of the finite element mass matrix on the dispersion characteristics of second-order wave equation for acoustic fluid–structure interaction. Christon and Voth [27, 28] have applied von Neumann analyses to assess the numerical performance of reproducing kernel semi-discretizations in one- and two-dimensions and considered both hyperbolic and parabolic partial differential equations.

In the ensuing discussion, Section 2 presents an overview of the generalized Fourier analysis used in this study to compute the phase and group speed, discrete and artificial diffusivity, and truncation error for the semi-discretizations. In Section 3, the phase and group speed, discrete diffusivity, and artificial diffusivity results are presented for the one-dimensional finite element, control-volume finite element, and finite difference/volume semi-discretizations. A complete summary of the one- and two-dimensional results may be found in Section 4 in Part II of this paper.

2. FORMULATION AND ANALYSIS

The starting point for the Fourier analysis is the linear advection–diffusion equation,

$$\frac{\partial T}{\partial t} + \nabla \cdot (\mathbf{u}T) = \alpha \nabla^2 T \tag{1}$$

Here, T is the temperature (or any other passive scalar), $\mathbf{u} = u\hat{\imath} + v\hat{\jmath}$ is the prescribed advective velocity, $\hat{\imath}$ and $\hat{\jmath}$ are unit vectors in the x and y-coordinate directions, respectively, and α is the thermal diffusivity. The advective velocity field is assumed to be div-free, i.e. $\nabla \cdot \mathbf{u} = 0$, in both the continuous and discrete sense. For the ensuing analysis, both the advective velocity and thermal diffusivity are constant.

Fourier analysis can be applied to spatially-discrete, temporally-discrete, and fully-discrete systems (where space and time are both discrete). For our purposes, we chose to consider the one- and two-dimensional semi-discrete equations which also correspond to the fully-discrete situation in the limit as $\Delta t \to 0$. The generic semi-discrete form of Equation (1) is

$$\mathbf{M}\dot{T} + \mathbf{A}(\mathbf{u})T + \mathbf{K}T = 0 \tag{2}$$

where $\mathbf{M}$ is a generalized unit-mass matrix, $\mathbf{A}(\mathbf{u})$ is the advection operator, and $\mathbf{K}$ is the diffusivity operator. The specifics of each of the generic operators and centering/averaging of the dependent variable, T, remains to be specified. The appendix presents the stencils for the various methods analysed in this work.

For a typical finite difference method, the generalized unit-mass matrix is simply the identity matrix, $\mathbf{I}$, and $\mathbf{K}$ is the standard five-point difference representation of the Laplacian. In this case, T represents grid-point (or cell-centered) values of the temperature. For the upwind methods, the advective operator and mass matrix vary according to the specific scheme under consideration.

For the finite element method, the generalized unit-mass matrix is

$$\mathbf{M} = \phi \mathbf{M}_{\mathrm{c}} + (1 - \phi)\mathbf{M}_{\mathrm{l}} \tag{3}$$

where $\mathbf{M}_{\mathrm{c}}$ is the consistent mass matrix, $\mathbf{M}_{\mathrm{l}}$ is the row-sum lumped (diagonal) mass matrix, and $0 \leqslant \phi \leqslant 1$. In this case, T represents node-centered temperature values. The details for obtaining the weak form of the advection–diffusion equation and the associated mass, advection and diffusion operators are well known (see for example Reference [8]), and are not repeated here.

We also consider several variants of a node-centered finite volume scheme and the control-volume finite element method in this work. The node-centered finite volume method uses a cell-averaged temperature, $\overline{T} = 1/V \int_V T \, \mathrm{d}V$ where V represents the cell volume centered at the node. Thus, in the results presented here, and in Part II of this paper, the finite volume results should be interpreted in terms of a cell-averaged temperature. In contrast, the control-volume finite element method relies on nodal temperatures.

2.1. Fourier analysis

The Fourier analysis proceeds by choosing either an infinite computational domain or alternatively a periodic domain. In the ensuing analysis, a 'regular' Cartesian grid is considered where the mesh spacing in the x and y-coordinate directions is Δx and Δy, respectively.

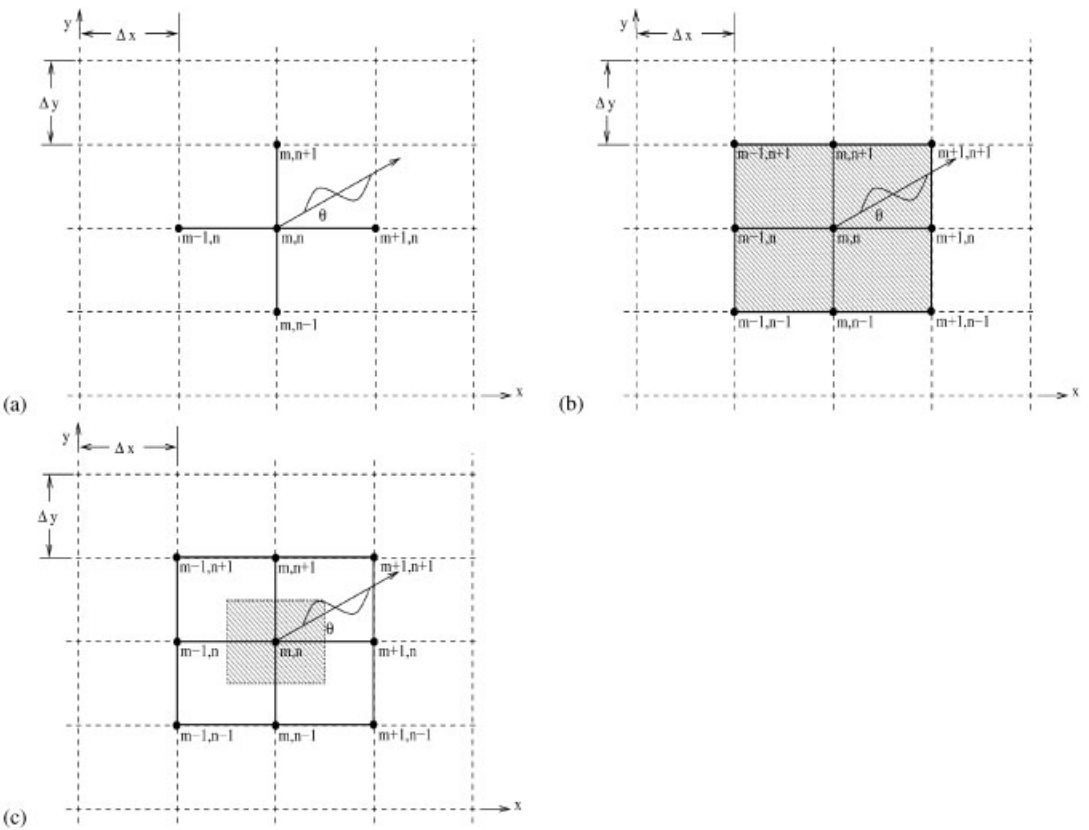

Figure 1. Propagation direction: (a) on a finite difference grid; (b) on a 2×2 patch of a finite element mesh; (c) on a control-volume finite element mesh.

This is illustrated in Figure 1(a) for a five-point finite difference stencil, Figure 1(b) for a patch of four quadrilateral finite elements, and Figure 1(c) for control-volume finite elements. The wave vector direction is denoted by θ, and the nodal x and y locations are given by $x_m = m\Delta x$, and $y_n = n\Delta y$, with the aspect ratio, $\gamma = \Delta y/\Delta x$.

Remark
The restriction to regular grid configurations does not restrict the application of the generalized Fourier analysis to only grids comprised of quadrilaterals. For example, regular arrangements of triangular elements may be analysed as in Reference [29].

A fundamental solution to the continuous problem is selected for a fixed wave number or wavelength and placed on the computational domain as shown in Figure 2. In general, the wave vector **k** and velocity vector **u** need not be aligned, but to simplify our two-dimensional analysis, we assume the wave vector and velocity vector are aligned, i.e. $\vartheta = \theta$. In Part II of this paper, the assumption that the wave vector and velocity vector are aligned is relaxed for one representative discretization method. However, practical space limitations prohibits extensive discussion of this additional effect.

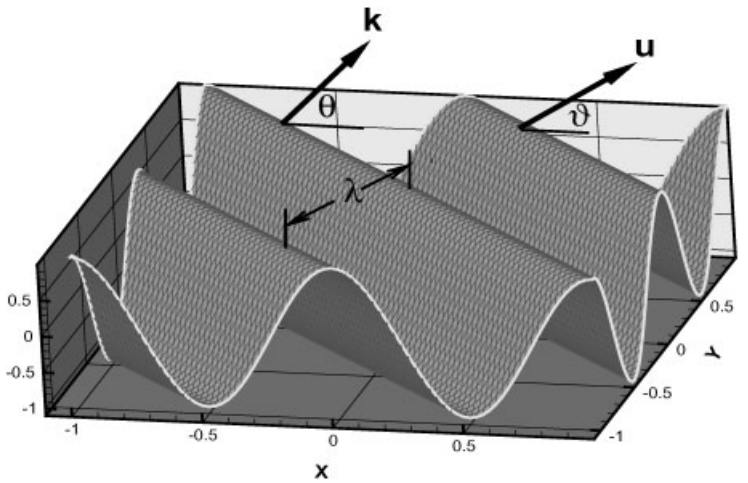

Figure 2. Fundamental solution with wavelength λ, advective velocity $\mathbf{u}$ and direction ϑ, and wave vector $\mathbf{k}$ and direction θ.

Using the fundamental solution, the response of the discrete system, discretized via finite differences, finite elements, etc. may then be computed in terms of the grid aspect ratio, mesh resolution, wave number, propagation speed and direction. The response of the discrete system is wavelength dependent, and is used to identify and characterize the phase and group speed, discrete thermal diffusivity, artificial diffusivity, grid bias, and asymptotic convergence rates.

Proceeding with the analysis and following Vichnevetsky and Bowles [4], we begin with a pure advection problem where

$$\mathbf{M}\left\{\frac{\mathrm{d}T}{\mathrm{d}t}\right\} + \mathbf{A}(\mathbf{u})T = 0 \tag{4}$$

and consider a sinusoidal trial solution of the form

$$T_{k,(m,n)}(t) = \hat{T}_k(t)\zeta(\mathbf{k},\mathbf{x}) \tag{5}$$

where $\zeta(\mathbf{k},\mathbf{x})$ is a column vector with entries for each (m,n) grid point corresponding to

$$\zeta(\mathbf{k},\mathbf{x}) = \left\{\begin{array}{c} \exp[\imath\mathbf{k}\cdot\mathbf{x}_{(1,1)}] \\ \vdots \\ \exp[\imath\mathbf{k}\cdot\mathbf{x}_{(m,n)}] \\ \vdots \\ \exp[\imath\mathbf{k}\cdot\mathbf{x}_{(M,N)}] \end{array}\right\} \tag{6}$$

Here, $\mathbf{k}$ is the wave vector, $k = \|\mathbf{k}\|$ is the wave number, $\mathbf{x}_{(m,n)} = x_m\hat{\imath} + y_n\hat{\jmath}$, and $\imath = \sqrt{-1}$. The grid location identified by (m,n) corresponds to $(x_m, y_n) = (m\Delta x, n\Delta y)$ with the total number of grid points in the x- and y-directions being (M,N), respectively.

We note in passing that by casting the semi-discrete equations on a Cartesian grid, the mass, advection and diffusivity matrices have a banded structure where the non-zero entries in the matrices are equal along lines parallel to the main diagonal, i.e. they are Toeplitz matrices.

Equation (5) is a solution to Equation (4) provided that

$$\frac{\mathrm{d}\hat{T}_k}{\mathrm{d}t} = \hat{A}(k)\hat{T}_k \tag{7}$$

where $\hat{A}(k)$ is the symbol (also referred to as the spectrum). The symbol is easily computed as

$$\hat{A}(k) = \frac{-\overline{\zeta}^{\mathrm{T}}\mathbf{A}(\mathbf{u})\zeta}{\overline{\zeta}^{\mathrm{T}}\mathbf{M}\zeta} \tag{8}$$

where the entries of $\overline{\zeta}$ are the complex conjugate of the entries in ζ, i.e. $\overline{\zeta}(\mathbf{k}, \mathbf{x}_{(m,n)}) = \exp[-\imath\mathbf{k}\cdot\mathbf{x}_{(m,n)}]$. Calculation of the symbol relies on the fact that $\overline{\zeta}^{\mathrm{T}}\mathbf{M}\zeta \neq 0$ which is the case for all of the methods considered here, i.e. the mass is either the identity, is symmetric, positive definite (SPD), or contains an SPD part. As noted by Vichnevetsky [4], $\zeta(\mathbf{k}, \mathbf{x})$ are the eigenvectors of the discrete Toeplitz operator $\mathbf{M}^{-1}\cdot\mathbf{A}(\mathbf{u})$, and $\hat{A}(k)$ are the corresponding eigenvalues.

The solution to Equation (4) at each grid point (m, n), found by direct integration, is

$$T_{k,(m,n)}(t) = \hat{T}_k(0)\,\exp[\mathrm{Re}(\hat{A}(k))t]\,\exp[\imath\{\mathbf{k}\cdot\mathbf{x}_{(m,n)} + \mathrm{Im}(\hat{A}(k))\}t] \tag{9}$$

where $\mathrm{Re}(\hat{A})$ is the real part of the symbol, and $\mathrm{Im}(\hat{A})$ is the imaginary part. A similar equation is true for the continuous advection equation. So, as demonstrated by Vichnevetsky [4], the sinusoidal trial solutions, with the proper time-dependent coefficients, are solutions to both the semi-discrete and continuous equations. Based on this fact, the difference between the continuous and semi-discrete solutions may be compared one wave number at a time in order to assess the artifacts introduced by the spatial discretization.

For the pure advection problem, there are two effects to be considered: dissipation and dispersion. The semi-discrete solution does not decay with time if

$$|\hat{T}_k(t)| = |\hat{T}_k(0)|\exp[\mathrm{Re}(\hat{A}(k))] \tag{10}$$

which can only be true if $\mathrm{Re}(\hat{A}(k)) = 0$. In this situation, the semi-discretization is said to be energy conserving. This is the case when $\mathbf{A}(\mathbf{u})$ is skew-symmetric and $\mathbf{M}$ is symmetric. In either case, when the amplitude of the signal does not decay with time, the semi-discretization is also referred to as neutrally dissipative.

In contrast, there is amplitude decay when at least some of the real eigenvalues are negative. That is, if $\mathrm{Re}(\hat{A}(k)) \leqslant 0$ for all k, or $\mathrm{Re}(\hat{A}(k)) < 0$ for some of k, then the amplitude of the solution will decay in time, and the semi-discretization is dissipative. The introduction of a non-symmetric $\mathbf{M}$ can result in a scheme that is dissipative even if $\mathbf{A}(\mathbf{u})$ is skew-symmetric. This is the situation for both FEM-SUPG and CVFEM-SUCV. If $\mathrm{Re}(\hat{A}(k)) > 0$ for some k, then the amplitude of the signal will grow in time, and the semi-discretization is considered to be unstable.

Remark
An alternative approach to the decomposition of the advection operator into symmetric and skew-symmetric parts proceeds as follows. Given an arbitrary advection operator, $\mathbf{A}$, the symmetric (diffusive) part is $\mathbf{A}_{\text{sym}} = 1/2(\mathbf{A} + \mathbf{A}^{\text{T}})$ and the skew-symmetric part is $\mathbf{A}_{\text{skew}} = 1/2(\mathbf{A} - \mathbf{A}^{\text{T}})$. Fourier analysis can, of course, be performed with these operators directly. However, the Fourier analysis will automatically perform an equivalent decomposition that yields the real and imaginary components of the symbol, $\hat{A}(k)$. The appendix presents the semi-discrete operators in a *stencil* format with the x and y-advection operators split into symmetric and skew-symmetric components for all of the methods considered in this paper.

When $\text{Re}(\hat{A}_k) = 0$, i.e. the discretization is energy conserving, and the only remaining numerical artifact is the difference between the speed that signals propagate in the continuous and discrete sense. In order to assess this effect, Equation (5) is written as

$$T_{k,(m,n)}(t) = \hat{T}_k(0)\ \exp[\imath k(m\Delta x \cos\theta + n\Delta y \sin\theta + \text{Im}(\hat{A}(k)t/k)] \tag{11}$$

By definition, the phase speed is the projection of $\mathbf{u} = \|\mathbf{u}\|(\cos\vartheta\hat{\imath} + \sin\vartheta\hat{\jmath})$ in the direction of $\mathbf{k}$,

$$c \equiv \frac{\mathbf{u}\cdot\mathbf{k}}{k} = \|\mathbf{u}\|\cos(\theta - \vartheta) \tag{12}$$

The cyclic frequency is

$$\omega = \mathbf{u}\cdot\mathbf{k} \tag{13}$$

which when substituted into Equation (12) yields the continuous phase speed,

$$c = \frac{\omega}{k} \tag{14}$$

As noted earlier, for the ensuing discussion we assume $\theta = \vartheta$ and so have $c = \|\mathbf{c}\| = \|\mathbf{u}\|$. This restriction is relaxed in Part II for one discretization to give a flavour of its effect.

From Equations (11) and (14), the discrete, or apparent phase speed is

$$\tilde{c}(k) = \frac{\tilde{\omega}}{k} = \frac{\text{Im}(\hat{A}(k))}{k} \tag{15}$$

where $\tilde{\omega}$ is the discrete analogue to ω. Equation (15) clearly shows the wave number dependence of the discrete phase velocity. Thus, it is clear that each wavelength will propagate at its own unique velocity on the computational grid.

The group velocity, $\mathbf{v_g} = v_{g_x}\hat{\imath} + v_{g_y}\hat{\jmath}$, often referred to as the energy velocity, describes how local disturbances that are modulated by a longer-wavelength signal propagate. The group velocity is defined as

$$\mathbf{v_g} = \frac{\partial\omega}{\partial k_x}\,\hat{\imath} + \frac{\partial\omega}{\partial k_y}\,\hat{\jmath} \tag{16}$$

where, $k_x = k\cos(\theta)$ and $k_y = k\sin(\theta)$. For a non-dispersive continuum the group velocity is simply the advective velocity, i.e. $v_{g_x} = u$ and $v_{g_y} = v$. In the discrete or dispersive case, the

group velocity is not always aligned with the wave vector, but instead has a propagation direction defined by

$$\Theta = \arctan\left(\frac{\tilde{v}_{g_y}}{\tilde{v}_{g_x}}\right) \tag{17}$$

where $\tilde{v}_{g_x} = \partial\tilde{\omega}/\partial k_x$, and $\tilde{v}_{g_y} = \partial\tilde{\omega}/\partial k_y$ are the components of the discrete group velocity.

Turning to the complete advection–diffusion problem, and following Vichnevetsky and Bowles [4] and Mullen and Belytschko [29], a general solution to Equation (1) is developed in the following form:

$$T(x, y, t) = A\exp[\imath k(x\cos\theta + y\sin\theta) - \imath\omega t - k^2\alpha t] \tag{18}$$

Here, k denotes the wave number, the wave vector is $\mathbf{k} = k\cos\theta\hat{\imath} + k\sin\theta\hat{\jmath}$, and ω is the circular frequency associated with the advective solution. The general solution in Equation (18) incorporates two fundamental solutions—one for the advective part, and one for the diffusive part of the advection–diffusion problem obtained by linear superposition.

Now, turning to the semi-discrete case, the general solution may be written in terms of the grid-spacing as

$$T_{m,n}(t) = A\exp[\imath k(m\Delta x\cos\theta + n\Delta y\sin\theta) - \imath\tilde{\omega}t - k^2\tilde{\alpha}t] \tag{19}$$

where $\tilde{\omega}$ is the discrete wavelength-dependent circular frequency, $\tilde{\alpha}$ is the discrete wavelength-dependent diffusivity, and the subscript k has been suppressed for notational convenience. After substitution into Equation (2), and using the appropriate stencils from the appendix, the result may be segregated into its real and imaginary components yielding relationships for the discrete circular frequency $\tilde{\omega}$, discrete phase speed $\tilde{c} = \tilde{\omega}/k$, and the discrete diffusivity $\tilde{\alpha}$. For a detailed example of this procedure for second-order upwind, see Reference [30].

2.2. *Asymptotic analysis*

In order to provide a basis for comparison between methods that are derived using Taylor series expansions and Galerkin based methods, which are not subservient to Taylor series, we make use of the relationship between Fourier analysis and classical truncation error analysis as pointed out by Vichnevetsky and Bowles [4, see pp. 24–26, 103–108]. The connection between Fourier analysis and truncation error provides the means to extract the leading-order of the truncation error for a method based on the asymptotic behaviour of the discrete phase error.

The methodology outlined by Vichnevetsky and Bowles begins with a definition of the classical truncation error, which given a solution to the one-dimensional continuous advection problem, $T(x,t)$, may be written as

$$\{\text{T.E.}\} = \left\{\frac{\mathrm{d}T_m}{\mathrm{d}t}\right\} - [\mathbf{M}^{-1}\mathbf{A}(\mathbf{u})]\{T_m\} \tag{20}$$

where $T_m(t) = T(x_m, t)$ are the values of $T(x,t)$ evaluated at the discrete points x_m.

Using a Taylor series expansion about grid point m, and substituting the results into Equation (20) the discretization error may be estimated in terms of the grid spacing Δx. For the semi-discretizations considered here, as demonstrated by Vichnevetsky and Bowles, a generalized model for the truncation error associated with the semi-discretization may be written as

$$\text{T.E.} = C\Delta x^p \left(\frac{\partial^{p+1} T}{\partial x^{p+1}} \right) + \text{H.O.T} \tag{21}$$

where C is a constant independent of the data, grid spacing Δx and formal order of accuracy p.

By taking the (spatial) Fourier transform of Equations (20) and (21) and equating the results, Vichnevetsky and Bowles obtained the following relationship between the discrete phase velocity, the continuous phase velocity and the truncation error,

$$\tilde{c} - c = C(\imath \Delta x k)^p + \text{H.O.T}^{\ddagger} \tag{22}$$

Rearranging, this may be cast as a phase error in Fourier space,

$$\frac{\tilde{c}}{c} - 1 = \hat{C}(\imath k \Delta x)^p + \text{H.O.T.} \tag{23}$$

i.e. an error-free discrete phase velocity would yield $\tilde{c}/c = 1$. As will be shown in Section 3.1, the order of accuracy may be recovered from the slope of the non-dimensional phase speed, $\tilde{c}/c$ as $k\Delta x \to 0$. Alternatively, the order of accuracy may be obtained by expanding the analytical formulae for the phase speed in terms of $k\Delta x$ and extracting the leading-order terms in the limit as $k\Delta x \to 0$. In the ensuing discussion, we make use of this relationship to identify the order of accuracy for the advective and diffusive discretizations considered in this work.

2.3. Semi-discrete methods

In this work, a variety of popular finite difference, finite volume and finite element methods are considered. The Fourier analysis used to develop the baseline methods comparison is restricted to analysis on 'regular' Cartesian grids—although we consider grids with non-unit aspect ratio in two dimensions. In the Cartesian grid setting many of the finite volume methods considered here revert to stencils that correspond to familiar finite difference methods. All of the semi-discrete operators for the methods considered in this work are presented in the appendix.

The family of finite volume methods considered are, in general, developed for unstructured grids using a combination of MUSCL [31] interpolation with slope limiters and gradient reconstruction methods to model the convection terms. Two methods of gradient reconstruction are considered: application of the divergence theorem and an unweighted least squares procedure [32]. As noted before, these finite volume methods rely on a cell-averaged temperature, $\overline{T}$. For the model problem under scrutiny, the node-centered finite volume results are based on the following semi-discrete equation which has been cast on a Cartesian grid

[‡]Note that the wave number k corresponds to ω in Equation (2.25) of Vichnevetsky and Bowles [4].

(see Figure 1),

$$\Delta x\Delta y\frac{\partial \overline{T}_{m,n}}{\partial t} + \Delta y u(T_{m+1/2,n} - T_{m-1/2,n}) + \Delta x v(T_{m,n+1/2} - T_{m,n-1/2})$$
$$= \alpha\frac{\Delta y}{\Delta x}(\overline{T}_{m+1,n} - 2\overline{T}_{m,n} + \overline{T}_{m-1,n}) + \alpha\frac{\Delta x}{\Delta y}(\overline{T}_{m,n+1} - 2\overline{T}_{m,n} + \overline{T}_{m,n-1}) \tag{24}$$

The various finite volume methods are derived by applying the generic MUSCL interpolation for convective terms, e.g.

$$T_{m+1/2,n} = \overline{T}_{m,n} + \frac{\psi}{2}[(1-\kappa)\nabla\overline{T}_{m,n}\cdot(\mathbf{r}_{m+1,n} - \mathbf{r}_{m,n}) + \kappa(\overline{T}_{m+1,n} - \overline{T}_{m,n})] \tag{25}$$

where $0 \leqslant \psi \leqslant 1$ is a slope limiter, and $\mathbf{r}_{m,n}$ is the position vector. In this work, the nonlinear aspects of this type of slope limiter are not considered. Instead, the two extrema for ψ are used, i.e. $\psi = 0$ and $\psi = 1$. The various finite volume methods are derived for different combinations of the parameter κ and the method of gradient reconstruction to compute $\nabla\overline{T}_{i,j}$ in the interpolation formula.

For Cartesian grids, application of the divergence theorem yields a central difference approximation for the cell gradients, which when substituted into the MUSCL interpolant yield semi-discretizations that correspond to a variety of well-known higher order difference methods for $\psi = 1$: second-order central-difference (CD, $\kappa = 1$), second-order upwind (SOU, $\kappa = -1$), Fromm [1] differencing (this is the limit of Fromm's fully discrete method for $\Delta t \to 0$; $\kappa = 0$), QUICK [33] ($\kappa = 1/2$), and a third-order upwind method (TOU) also due to Leonard [33] ($\kappa = 1/3$). Note that the version of QUICK considered here neglects the transverse-curvature terms required to obtain uniform third-order accuracy for advection—see Equation (30) in Leonard [34]. We also consider an *ad hoc* method composed of CD with a 'finite element like' consistent mass matrix that can be derived by assuming a linear variation of the field variable within the control volume.

We analyze two finite volume schemes derived using the unweighted least-squares reconstruction and $\kappa = -1$ and 0. For convenience we will refer to these as LSR(-1) and LSR(0) in the subsequent sections. Note that in one space dimension, the LSR(-1) scheme corresponds to the second-order upwind (SOU) method, and the LSR(0) scheme corresponds to Fromm's method. However, in two space dimensions, this is not the case.

For the finite element methods, we consider the well-known Galerkin finite element method (FEM) and its streamline-upwind Petrov–Galerkin (FEM-SUPG) derivative along with the more recently developed control volume finite element method (CVFEM) and its analogue to SUPG, known as SUCV (CVFEM-SUCV) [2, 3].

3. RESULTS

In this section, a summary of the discrete phase speed, group speed, diffusivity and artificial diffusivity is presented. The asymptotic truncation error associated with the phase and group speed, discrete and artificial diffusivity is presented for each method along with the resolution requirements for 5 and 1% error levels in the phase speed. In the discussion that follows, the

numerical approximation to the physical diffusivity α is referred to as the discrete diffusivity $\tilde{\alpha}$, and the diffusivity added directly or indirectly by the advection scheme is referred to as the artificial diffusivity α_{art}. The non-dimensional phase speed ($\tilde{c}/c$), group speed ($\tilde{v}_g/c$), discrete diffusivity ($\tilde{\alpha}/\alpha$), and artificial diffusivity ($1/\mathbf{P}_e^{\text{art}}$) are presented as functions of the non-dimensional wave number, $2\Delta x/\lambda = k\Delta x/\pi$. The grid Peclet number is defined as $\mathbf{P}_e = c\Delta x/2\alpha$, and the Peclet number based on the artificial diffusivity is defined as $\mathbf{P}_e^{\text{art}} = c\Delta x/2\alpha_{\text{art}}$. For simplicity, the non-dimensional results are referred to as the phase, group, discrete diffusivity and artificial diffusivity.

Remark
An alternative and equivalent non-dimensional scaling for the artificial diffusivity is based on the physical diffusivity, i.e. $\alpha_{\text{art}}/(\alpha\mathbf{P}_e)$. However, this definition is equivalent to the scaling defined above and requires the introduction of a physical diffusivity which need not be present in the case of pure advection (although the artificial diffusivity may always be present). In addition, for the limiting case of pure advection where $\mathbf{P}_e \to \infty$, defining $\mathbf{P}_e^{\text{art}} = c\Delta x/2\alpha_{\text{art}}$ provides an indicator of how much the discrete solution deviates from pure advection. In addition, this metric indicates that when artificial diffusivity is introduced, the apparent or effective Peclet number will remain finite—at least through a portion of the discrete spectrum.

For each numerical method, the analytical expressions for the phase and group speed, discrete and artificial diffusivity are presented in a compact form as an aid to understanding the results of the Fourier analysis (see Tables II, IV, VI, and VIII). In the analytic expressions for phase and group speed, discrete and artificial diffusivity, the influence of the mass matrix in the FEM, FEM-SUPG, CVFEM, and CVFEM-SUCV methods is expressed in terms of the function $\mathscr{M}(k\Delta x)$ as shown in Table I. Note that the second-order node-centered finite difference scheme with a consistent mass matrix, referred to as the CD-$\mathbf{M}_c$ method in subsequent sections, is identical to the CVFEM formulation in one dimension—although it is node-centered. Therefore, only the CVFEM results are presented here since the equivalent semi-discrete operators yield identical results. In addition, for the one-dimensional results, the second-order upwind (SOU) semi-discretization corresponds identically to the LSR(-1) scheme, and Fromm's method to the LSR(0) scheme. For this reason, we present results using the SOU and Fromm's labels in the one-dimensional results. However, we remind the reader that results for the LSR schemes should be interpreted in terms of a cell-averaged temperature and note that there can be significant differences in the details of the truncation error associated with FDM and FVM discretizations as pointed out by Leonard [35].

As a final note, we consider errors in phase, group and diffusivity of less than 1% to be small. For the purposes of our discussion, errors between 1 and 5% are termed moderate while those that exceed 5% are deemed large. Note that this choice of error bounds is subjective,

Table I. Mass matrix contribution for FEM and CVFEM methods where $\mathbf{M}_l$ indicates a lumped mass matrix and $\mathbf{M}_c$ indicates a consistent mass matrix.

Method	$\mathscr{M}(k\Delta x)$
FEM/CVFEM-$\mathbf{M}_l$	1
FEM-$\mathbf{M}_c$	$(2+\cos(k\Delta x))/3$
CVFEM-$\mathbf{M}_c$	$(3+\cos(k\Delta x))/4$

Table II. Formulae for one-dimensional phase speed.

Method	Phase speed ($\tilde{c}/c$)
FOU	$\sin(k\Delta x)/k\Delta x$
SOU	$[4\sin(k\Delta x) - \sin(2k\Delta x)]/2k\Delta x$
TOU	$[8\sin(k\Delta x) - \sin(2k\Delta x)]/6k\Delta x$
QUICK	$[10\sin(k\Delta x) - \sin(2k\Delta x)]/8k\Delta x$
Fromm's	$[6\sin(k\Delta x) - \sin(2k\Delta x)]/4k\Delta x$
FEM/CVFEM	$\dfrac{\sin(k\Delta x)[\mathscr{M}(k\Delta x) + \beta(2\beta + \mathbf{P}_e^{-1})(1 - \cos(k\Delta x))]}{k\Delta x(\mathscr{M}^2(k\Delta x) + \beta^2\sin^2(k\Delta x))}$

and further, depends upon the application of interest. However, in our experience, errors in phase, group and discrete diffusivity of less than 5% are acceptable for many engineering applications.

3.1. Phase speed

The analytic expressions for the non-dimensional phase speed for all of the semi-discrete methods considered may be found in Table II. Here, the compact notation for the mass matrix (see Table I) is used for the FEM/CVFEM phase speed. The stabilized methods (FEM-SUPG and CVFEM-SUCV) introduce a $\mathbf{P}_e$ number dependence in the phase speed as indicated by the presence of the stabilization parameter, β (see the appendix, Equation (A28)), and the Peclet number $\mathbf{P}_e$. Here, the FEM and CVFEM phase speeds are recovered for $\beta = 0$. The phase speed formulae for second-order central differences, the Galerkin finite element method and control-volume finite element method may be found in Reference [8].[§]

The non-dimensional phase speed results for a variety of finite difference (or node-centered finite volume) methods are presented in Figure 3. For comparison, the non-dimensional phase speed for the FEM and CVFEM methods are presented in Figures 4 and 5. The phase speed for the FEM-SUPG and CVFEM-SUCV methods are also presented in Figures 4–6 for pure advection, i.e. when $\mathbf{P}_e \to \infty$.

In the absence of phase errors, the ideal semi-discrete phase speed would exactly replicate the continuous phase speed over the entire discrete spectrum from the limit $\Delta x \to 0$ to the grid Nyquist limit where $2\Delta x/\lambda = 1$. However, all of the methods considered here introduce phase errors—either lagging or leading, with signals associated with the Nyquist limit, i.e. $2\Delta x$ wavelengths, being stationary. In the one-dimensional limit, the lumped mass FEM and CVFEM, and FDM methods yield identical spatial discretizations and non-dimensional phase speed results.

Remark

In this initial multi-methods comparison, we have not considered the effects of *ad hoc* 'tricks-of-the-trade', such as reduced integration for the FEM and CVFEM formulations, on the phase

[§]The formula in Reference [8] for phase speed (Equations (2)–(9)) contains a typographical error in the numerator.

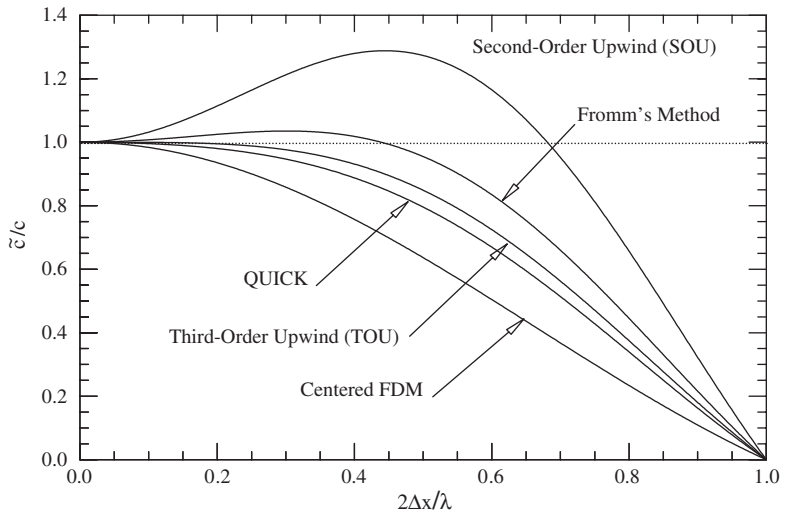

Figure 3. Non-dimensional phase speed for a variety of finite-difference (node-centered finite-volume) methods.

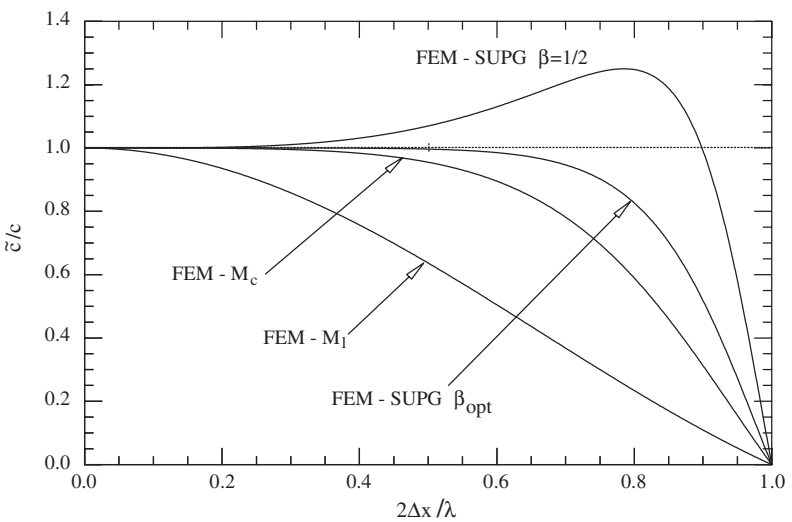

Figure 4. Non-dimensional phase speed for finite element method with a consistent mass matrix (FEM-$\mathbf{M}_c$), lumped mass (FEM-$\mathbf{M}_l$), consistent mass matrix and SUPG (FEM-SUPG) with β_{opt} and $\beta = \frac{1}{2}$.

and group speed, discrete and artificial diffusivity. The interested reader may consult Gresho *et al.* [36] who has considered the effects of reduced integration for the advection–diffusion equation using a Galerkin finite element formulation.

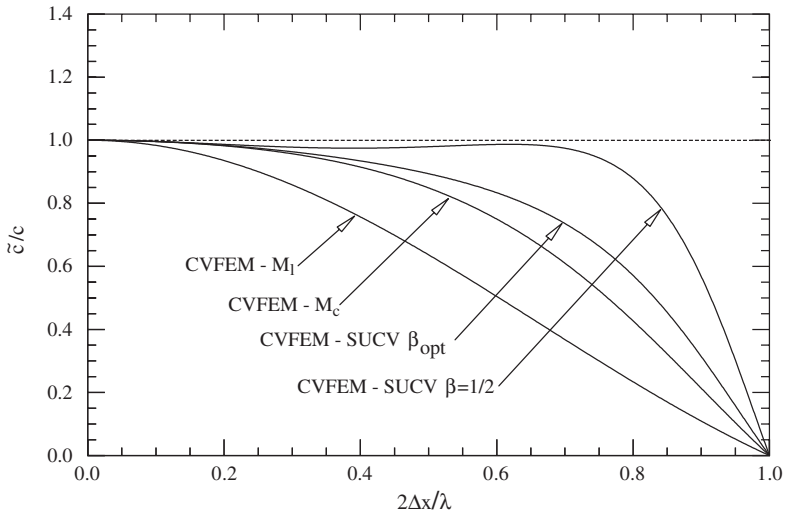

Figure 5. Non-dimensional phase speed for control-volume finite element method with a consistent mass matrix (CVFEM-$\mathbf{M}_c$), lumped mass (CVFEM-$\mathbf{M}_l$), and a consistent mass matrix and SUCV (CVFEM-SUCV) with β_{opt} and $\beta = \frac{1}{2}$.

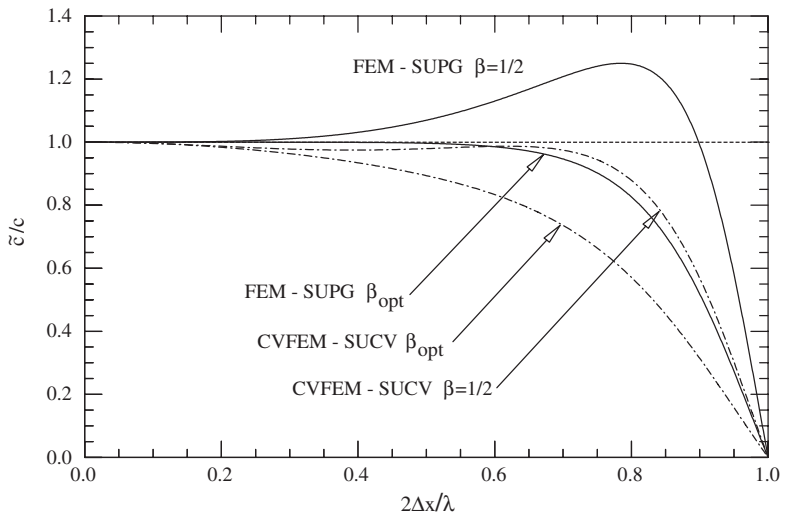

Figure 6. Non-dimensional phase speed for control-volume finite element and finite element methods using streamline upwinding (CVFEM-SUCV and FEM-SUPG).

As a reminder to the reader, recall that the first-order upwind scheme may be decomposed into a centered second-order advection scheme with concomitant second-order artificial viscosity. This is reflected in Figure 3 by the non-dimensional phase curve for the 'Centered FDM' scheme. Both Fromm's method and the SOU scheme introduce leading phase error

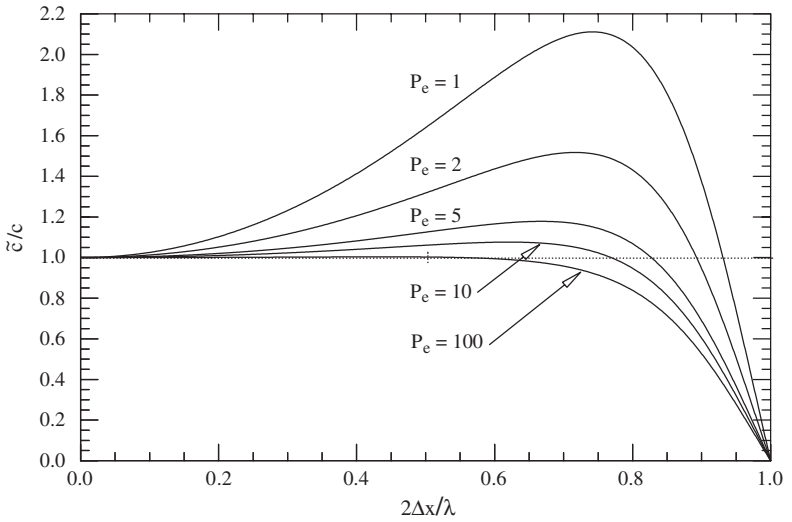

Figure 7. Non-dimensional phase speed for finite element method with a consistent mass matrix and FEM-SUPG with β_{opt} for $\mathbf{P}_e = 1,\ 2,\ 5,\ 10,\ 100$.

for the mid-range wavelengths although the severe ($\approx 30\%$) phase errors in the mid-range of the discrete spectrum for the second-order upwind method are significantly greater than for Fromm's method.

In comparison to the finite difference schemes, the only finite element formulation that yields leading phase errors as large as the second-order upwind scheme is the FEM-SUPG method with a constant stabilization parameter of $\beta = \frac{1}{2}$ (see Figure 4). Of interest here is the significant improvement in phase speed in moving from the baseline Galerkin FEM discretization using a consistent mass to the FEM-SUPG formulation with an optimal stabilization parameter $\beta_{\text{opt}} = 1/\sqrt{15}$. This value of the stabilization parameter was shown by Raymond and Gardner [37] to annihilate all truncation error up to sixth order; see Reference [8].

The CVFEM methods considered here yield strictly lagging phase error as shown in Figure 5. The CVFEM-SUCV method with β_{opt} (optimal β for FEM-SUPG) and a consistent mass matrix yields a non-dimensional phase speed close to the Galerkin FEM with a consistent mass matrix in the mid-range wavelengths. Although, it will be shown that CVFEM-SUCV cannot reproduce the fourth-order phase accuracy of the simple Galerkin FEM. The *ad hoc* application of the streamline-upwind Petrov–Galerkin formulation also cannot be 'tuned' to yield the high-order behaviour associated with FEM-SUPG. In fact, $\beta = \frac{1}{2}$ appears to be an overall better stabilization parameter for SUCV, albeit with noticeable lagging errors in the phase speed through the mid-range wavelengths of the discrete spectrum. A direct comparison between the FEM-SUPG and CVFEM-SUCV methods may be seen in Figure 6 where the lagging phase errors of the CVFEM-SUCV method are evident—even for the 'optimal' CVFEM-SUCV stabilization parameter, $\beta = \frac{1}{2}$.

The FEM-SUPG and CVFEM-SUCV methods exhibit a dependence on the Peclet number as shown in Figures 7 and 8 for $1 \leqslant \mathbf{P}_e \leqslant 100$ and optimal stabilization parameters—$\beta = 1/\sqrt{15}$ for FEM-SUPG and $\beta = \frac{1}{2}$ for CVFEM-SUCV. Both FEM-SUPG and CVFEM-SUCV yield

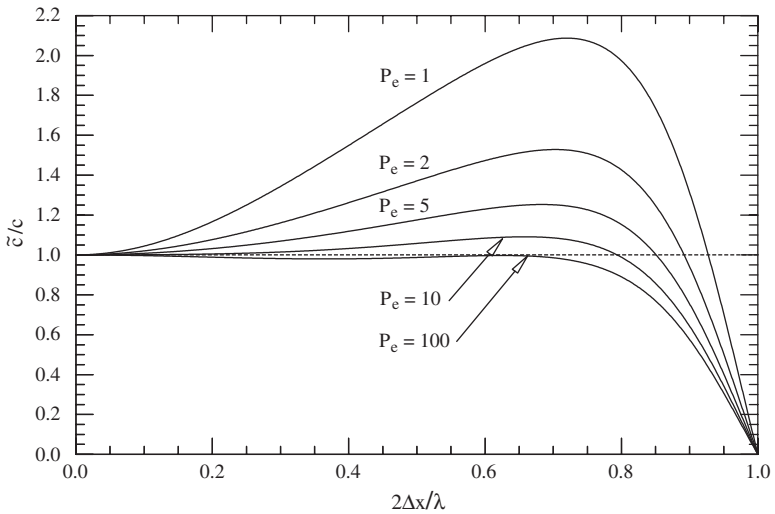

Figure 8. Non-dimensional phase speed for control-volume finite element method with a consistent mass matrix and CVFEM-SUCV with $\beta = \frac{1}{2}$ for $\mathbf{P}_e = 1,\ 2,\ 5,\ 10,\ 100$.

large leading phase errors over 50% or more of the discrete spectrum for $\mathbf{P}_e < 5$ suggesting that the stabilization parameter should be selected based on the Peclet number.

The deleterious effect of the Peclet number dependence may be ameliorated by using the stabilization parameter suggested by Brooks and Hughes [38] which in one dimension is

$$\tau = \beta \frac{\Delta x \xi}{u} \tag{26}$$

where

$$\xi = \coth(\mathbf{P}_e) - \frac{1}{\mathbf{P}_e} \tag{27}$$

Figure 9 shows that ξ approaches unity for large Peclet number and goes to zero rapidly for $\mathbf{P}_e \leqslant 3$. Tezduyar [39] has suggested a doubly-asymptotic approximation to ξ as a more computationally efficient alternative to Equation (27). The influence of the Peclet-adjusted stabilization on the phase speed is shown in Figure 10 for FEM-SUPG and in Figure 11 for CVFEM-SUCV. In both cases, moderate to large leading phase errors are introduced in the mid-range of the discrete spectrum.

3.1.1. Asymptotic truncation error and resolution estimates. The asymptotic truncation error in phase speed can be determined by taking the limit as $k\Delta x \to 0$ in the analytical expressions given in Table II. Asymptotic representations for SOU, Fromm, TOU and QUICK are given by

$$\frac{\tilde{c}}{c} \sim 1 - \frac{1}{6}\frac{n-8}{n-2}(k\Delta x)^2 + O((k\Delta x)^4) \tag{28}$$

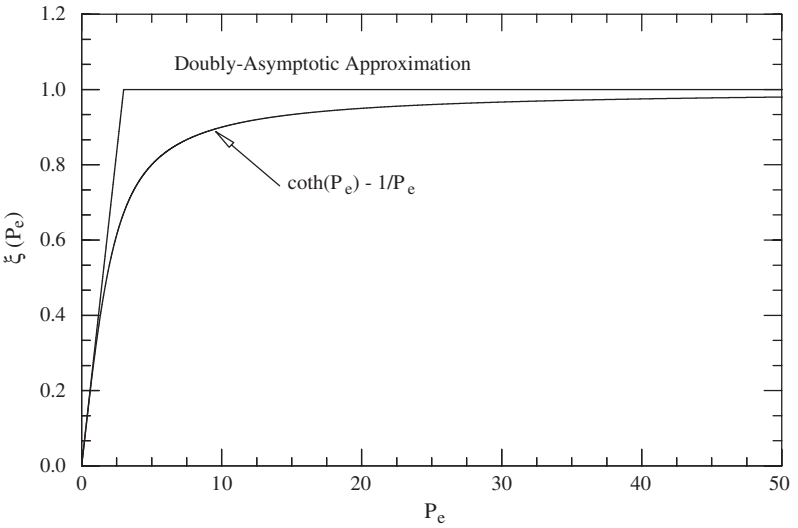

Figure 9. Doubly-asymptotic stabilization parameter for FEM-SUPG—see Reference [39].

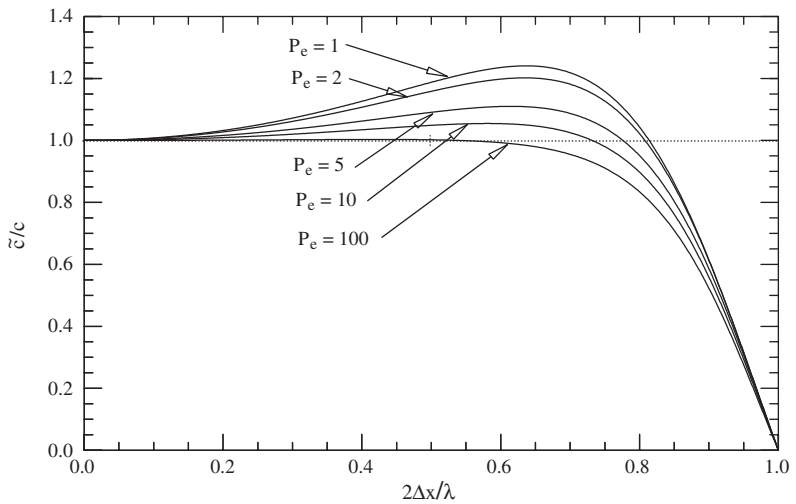

Figure 10. Non-dimensional phase speed for the finite element method with a consistent mass matrix and FEM-SUPG using β_{opt} and $\xi = \coth(\mathbf{P}_e) - 1/\mathbf{P}_e$ for $\mathbf{P}_e = 1,\ 2,\ 5,\ 10,\ 100$.

for $n = 4$, 6, 8, and 10, for each of these methods, respectively. These methods are second-order, except for TOU which is fourth order (with a leading coefficient of $-1/30$). The asymptotic results for the upwind finite volume/finite difference methods may be verified by forming the Taylor series approximations for the skew-symmetric parts of the advection operators.

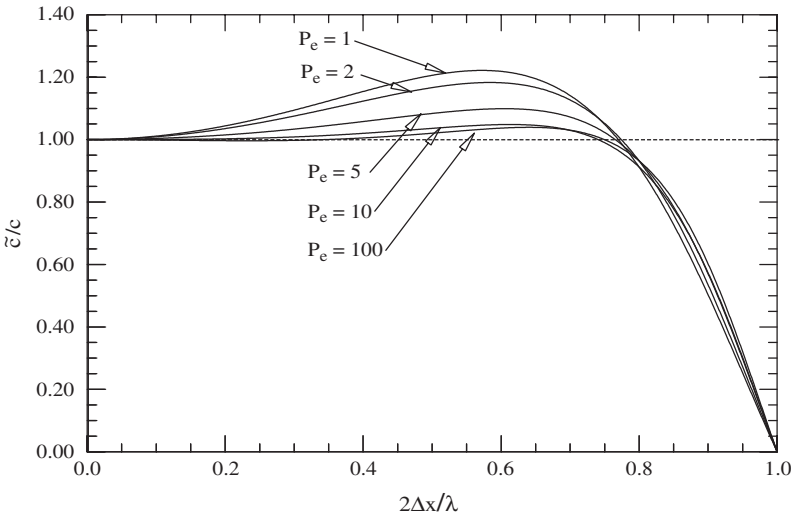

Figure 11. Non-dimensional phase speed for control-volume finite element method with a consistent mass matrix and SUCV with $\beta = \frac{1}{2}$ and $\xi = \coth(\mathbf{P}_e) - 1/\mathbf{P}_e$ for $\mathbf{P}_e = 1, 2, 5, 10, 100$.

Remark
The first-order upwind scheme yields a centered skew-symmetric second-order advection operator, and consequently the asymptotic estimate for the truncation error based on the phase speed yields $O(\Delta x^2)$.

For both FEM-SUPG and CVFEM-SUCV the asymptotic representation of the non-dimensional phase speed has the form

$$\frac{\tilde{c}}{c} \sim 1 + g_2(k\Delta x)^2 + g_4(k\Delta x)^4 + O((k\Delta x)^6) \tag{29}$$

In the limit of pure advection, i.e. $\mathbf{P}_e \to \infty$, $g_2 \equiv 0$ as shown by Gresho and Sani [8] (see Equation (2.6)–(180)) for FEM-SUPG. By choosing $\beta = 1/\sqrt{15}$,

$$g_4 = \frac{\beta^2}{12} - \frac{1}{180} \tag{30}$$

can also be made zero resulting in a sixth-order accurate method.

For CVFEM-SUCV g_2 is independent of β, with an asymptotic representation of

$$\frac{\tilde{c}}{c} \sim 1 - \frac{1}{24}(k\Delta x)^2 + \left(\frac{\beta^2}{8} - \frac{7}{960}\right)(k\Delta x)^4 + O((k\Delta x)^6) \tag{31}$$

Therefore for CVFEM-SUCV there is no β that will result in a higher order formula or optimal phase speed behaviour in terms of $k\Delta x$. However, a heuristically optimal value of $\beta = \frac{1}{2}$ gives a dispersion curve that approaches FEM-SUPG (see Figures 8 and 7) although the truncation error is only $O(\Delta x^2)$ and there are lagging errors in the mid-range wavelengths.

Table III. Asymptotic estimates of truncation error and resolution requirements based on the phase error for pure advection.

Method	Asymptotic T.E.	$\lambda/\Delta x$ for 5% error	$\lambda/\Delta x$ for 1% error
FOU	$O(\Delta x^2)$	11.4	25.6
SOU	$O(\Delta x^2)$	15.8	36.2
TOU	$O(\Delta x^4)$	5.46	8.35
QUICK	$O(\Delta x^2)$	6.83	13.5
Fromm's	$O(\Delta x^2)$	3.96	17.4
FEM-$\mathbf{M}_c$	$O(\Delta x^4)$	3.93	5.61
FEM-$\mathbf{M}_l$	$O(\Delta x^2)$	11.4	25.6
FEM-SUPG β_{opt}	$O(\Delta x^6)$	2.88	4.76
FEM-SUPG $\beta = \frac{1}{2}$	$O(\Delta x^4)$	4.39	6.78
CVFEM-$\mathbf{M}_c$	$O(\Delta x^2)$	6.24	13.1
CVFEM-$\mathbf{M}_l$	$O(\Delta x^2)$	11.4	25.6
CVFEM-SUCV β_{opt}	$O(\Delta x^2)$	5.71	12.8
CVFEM-SUCV $\beta = \frac{1}{2}$	$O(\Delta x^2)$	2.69	11.8

Note that the FEM-SUPG and CVFEM-SUCV results are presented only for a consistent mass matrix $\mathbf{M}_c$.

If the lumped-mass approximation is applied to either FEM-SUPG or CVFEM-SUCV, i.e. row-sum-lumping of the original symmetric mass matrix, and not the skew-symmetric portion induced by the stabilization, the asymptotic truncation error reverts to,

$$\frac{\tilde{c}}{c} \sim 1 - \frac{1}{6}(k\Delta x)^2 + \left(\frac{\beta^2}{4} + \frac{1}{120}\right)(k\Delta x)^4 + O((k\Delta x)^6) \tag{32}$$

which for $\beta = 0$ gives the formula for the centered finite difference scheme (equivalent to lumped mass FEM and CVFEM).

The asymptotic convergence rates based on the phase error are presented in Table III. Figure 12 shows the slope of the phase error in the asymptotic range for the finite difference schemes considered here. We note that while the constant varies for the centered, second-order upwind, QUICK and Fromm's method, the slope of all these methods corresponds to a $O(\Delta x^2)$ convergence rate. Again, the third-order upwind method exhibits $O(\Delta x^4)$ convergence—a superconvergent behaviour that is still not clear to us.

In contrast to the finite difference results, the phase error for the finite element methods shown in Figure 13 indicate super-convergent behaviour except when a lumped mass matrix is used. The $O(\Delta x^6)$ behaviour of FEM-SUPG with the phase error minimizing stabilization parameter is clearly shown here, while $\beta = \frac{1}{2}$ is similar to the baseline Galerkin FEM results. The strictly second-order behaviour of CVFEM is shown by the phase-error plots in Figure 14. Unlike SUPG for the finite element method, the SUCV methods do not exhibit any reduction in phase error relative to the baseline CVFEM method with a consistent mass matrix. As with the finite element method, mass lumping increases the phase error, but for CVFEM there is no reduction in convergence rate as CVFEM does not exhibit any superconvergent behaviour.

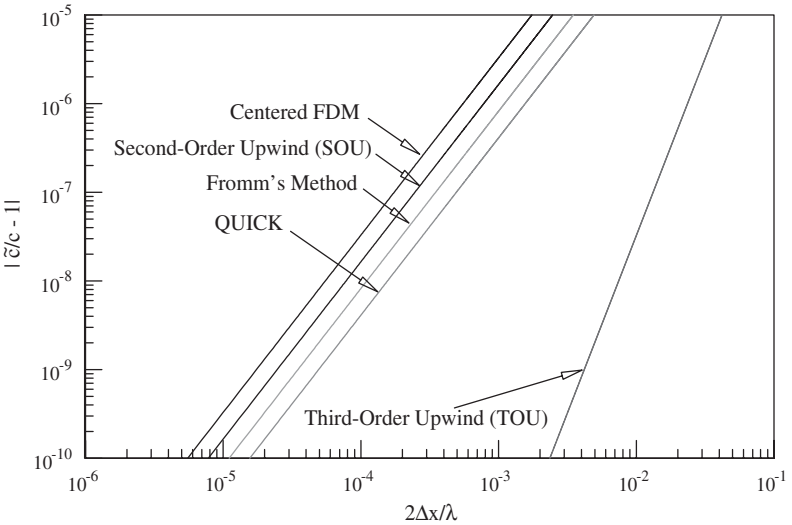

Figure 12. Asymptotic convergence rates based on phase error for a variety of finite-difference (node-centered finite-volume) methods.

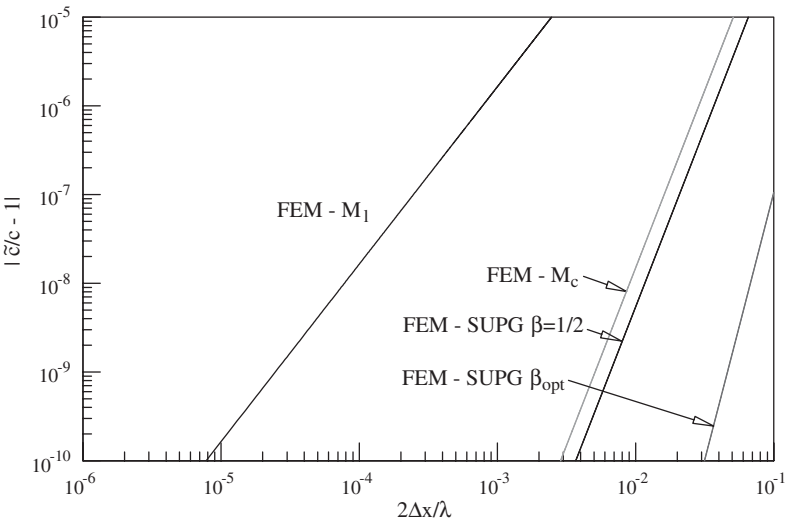

Figure 13. Asymptotic convergence rates based on phase error for the finite element method with a consistent mass matrix (FEM-$\mathbf{M}_c$), lumped mass (FEM-$\mathbf{M}_l$), consistent mass matrix and FEM-SUPG with β_{opt} and $\beta = \frac{1}{2}$.

In addition to the asymptotic truncation error, the phase error analysis may be used to estimate the required resolution for a given level of 'acceptable' error. The resolution requirements for a 5 and 1% error in phase are shown with the asymptotic truncation error estimates in Table III. Estimates for resolution requirements for additional finite difference methods may

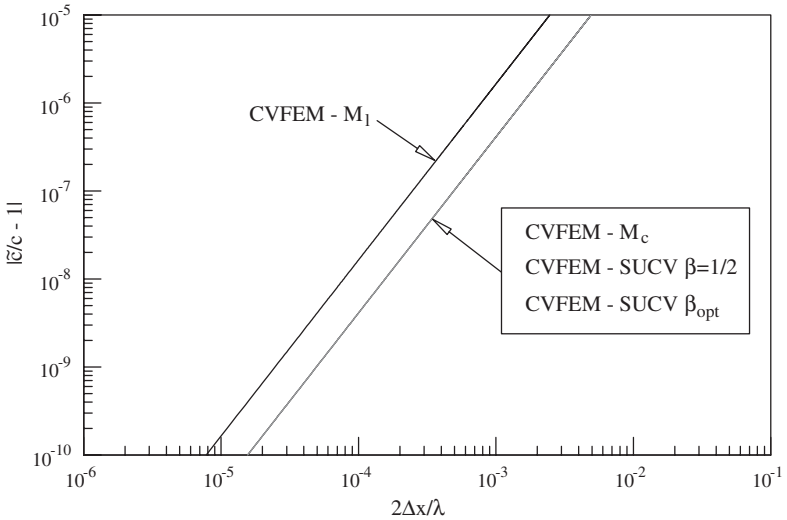

Figure 14. Asymptotic convergence rates based on phase error for the control-volume finite element method with a consistent mass matrix (CVFEM-$\mathbf{M}_c$), lumped mass (CVFEM-$\mathbf{M}_l$), consistent mass matrix and CVFEM-SUCV with β_{opt} and $\beta = \frac{1}{2}$.

be found in Reference [8, p. 155]. The best phase accuracy for the least grid resolution is provided by FEM-SUPG with β_{opt} while the worst case is the second-order upwind method which, despite its second-order accuracy, requires more resolution than the first-order upwind method for an equivalent error.

Although the CVFEM variants yield competitive resolution estimates for a 5% phase error, as the error band is tightened, the CVFEM methods do not perform as well as their FEM counterparts. This is due to the large lagging phase error through the midrange of the discrete spectrum (see Figure 5) which results in an increase in the resolution requirement by a factor of 3–5 relative to the finite element method. In a similar fashion, Fromm's method requires less resolution than TOU for a 5% phase error. However, for a 1% error in phase, the converse is observed—TOU requires less resolution per unit wavelength than Fromm's method. This reversal in resolution requirements is due to the fact that Fromm's method exhibits leading phase error for $0 \leqslant 2\Delta x/\lambda \leqslant 1/2$ that is less than 5%. Consequently, the resolution estimate for Fromm's method is based on the intersection of the phase error curve with $\tilde{c}/c = 0.95$ yielding a relaxed resolution estimate relative to TOU. A tighter error band of 1% captures the leading phase error resulting in the increased resolution estimate for Fromm's method in comparison to TOU. The result is a resolution requirement that is greater than twice that required for TOU as shown in Table III.

3.2. *Group speed*

In one-dimension, the non-dimensional group velocity is

$$\tilde{v}_g = \frac{\partial \tilde{\omega}}{\partial k} \tag{33}$$

For a non-dispersive medium, the group velocity is identical to the phase speed. However, as already discussed, the discretization procedures considered here result in a dispersive representation of the continuum problem, i.e. the phase speed is a function of the wave number. Thus, using Equation (14), Equation (33) may be written in terms of the wavelength-dependent phase speed as

$$\tilde{v}_g = \tilde{c}(k) + k \frac{\partial \tilde{c}}{\partial k} \tag{34}$$

Therefore, the group speed will only be identical to the phase speed, the ideal situation, when

$$k \frac{\partial \tilde{c}}{\partial k} = 0 \tag{35}$$

This can occur in the limit as $k \to 0$, i.e. a constant mode, or when the slope of the phase curve with respect to the wave number is zero—a situation that we desire in the limit of $k \to 0$.

Indeed, methods like FEM and FEM-SUPG with a consistent mass matrix and the associated higher-order phase speed accuracy do a good job of emulating this behaviour, but fail at the short wavelengths where the slope of the phase speed curve changes rapidly as the phase speed goes to zero with $2\Delta x/\lambda \to 1$, i.e. at the Nyquist limit. The consequence of this is reflected in the group speed which will become large and negative at the grid Nyquist limit. Thus, the better the phase speed behaviour through the discrete spectrum, the worse the group speed will be for $2\Delta x$ wavelengths. This is reflected in the results that follow.

The group speed results for all the methods considered here are shown in Table IV. The non-dimensional group speed for the finite difference methods, FEM and CVFEM are presented in Figures 15–17, respectively. As expected, all of the methods considered here exhibit relatively large negative group speed for $2\Delta x$ wavelengths. The large leading phase errors for the second-order upwind (SOU) method are reflected in the large (relative to the other FD methods) leading group errors and the large negative group speed at the grid Nyquist limit. The negative group speed at the Nyquist limit is a direct consequence of the fact that the phase speed decreases rapidly with respect to wave number as the Nyquist limit is approached.

For SOU, the leading phase error in the mid-range of the discrete spectrum leads to larger group errors for $0.7 \leqslant 2\Delta x/\lambda \leqslant 1.0$ relative to the other finite difference methods. Similar effects are observed in general for the FEM and CVFEM methods, but are somewhat more pronounced for the consistent mass and SUPG/SUCV variants. Again, this is due to the fact that phase speed remains faithful to the physical phase velocity over a larger range of the discrete spectrum. For the FEM-SUPG method with $\beta = \frac{1}{2}$, $\tilde{v}_g/c = -12$ for the $2\Delta x$ wavelengths. The phase-error-minimizing value of the stabilization parameter, $\beta_{\text{opt}} = 1/\sqrt{15}$ reduces this large negative group velocity at the Nyquist limit.

Although not shown here due to space limitations, the effect of the Peclet number scaling on SUCV and SUPG is to reduce the large negative group speed for $\mathbf{P}_e \leqslant 2$ relative to the case where scaling is not used. The reader is directed to Reference [30] for additional details.

3.2.1. Asymptotic truncation error and resolution estimates. The asymptotic truncation error in the group speed can be determined by taking the limit as $k\Delta x \to 0$ in the analytical expressions given in Table IV. The first- and second-order upwind methods are both $O(\Delta x^2)$

Table IV. Formulae for one-dimensional phase speed.

Method	Group speed ($\tilde{\vartheta_g}/c$)
FOU	$\cos(k\Delta x)$
SOU	$2\cos(k\Delta x) - \cos(2k\Delta x)$
TOU	$\frac{1}{3}[4\cos(k\Delta x) - \cos(2k\Delta x)]$
QUICK	$\frac{1}{4}[5\cos(k\Delta x) - \cos(2k\Delta x)]$
Fromm's	$\frac{1}{2}[3\cos(k\Delta x) - \cos(2k\Delta x)]$
FEM	$\frac{3(1+2\cos(k\Delta x))}{(2+\cos(k\Delta x))^2}$
FEM-SUPG	$\frac{[\mathscr{M}(k\Delta x)+(2\beta^2+\beta/\mathbf{P}_e)(1-\cos(k\Delta x))][\frac{4}{9}+\frac{1}{12}(7-3\beta^2)\cos(k\Delta x)+\frac{(9\beta^2-1)}{36}\cos 3(k\Delta x)]}{(\mathscr{M}^2(k\Delta x)+\beta^2\sin^2(k\Delta x))^2} + \left(\frac{\beta}{\mathbf{P}_e}+2\beta^2-\frac{1}{3}\right)\frac{\sin^2((k\Delta x))}{\mathscr{M}^2(k\Delta x)+\beta^2\sin^2(k\Delta x)}$
CVFEM	$\frac{4(1+3\cos(k\Delta x))}{(3+\cos(k\Delta x))^2}$
CVFEM-SUCV	$\frac{[\mathscr{M}(k\Delta x)+(2\beta^2+\beta/\mathbf{P}_e)(1-\cos(k\Delta x))]\left[\frac{3}{8}+\frac{(41-16\beta^2)}{64}\cos(k\Delta x)+\frac{(16\beta^2-1)}{64}\cos 3(k\Delta x)\right]}{(\mathscr{M}^2(k\Delta x)+\beta^2\sin^2(k\Delta x))^2} + \left(\frac{\beta}{\mathbf{P}_e}+2\beta^2-\frac{1}{4}\right)\frac{\sin^2((k\Delta x))}{\mathscr{M}^2(k\Delta x)+\beta^2\sin^2(k\Delta x)}$

in group speed. The asymptotic form of the group speed for Fromm, TOU and QUICK is

$$\frac{\tilde{v}_g}{c} \sim 1 + \frac{1}{2}\frac{4-n}{n-1}(k\Delta x)^2 + O((k\Delta x)^4) \tag{36}$$

for $n=3$, 4 and 5, respectively. Thus, Fromm and QUICK are also second order in group, while TOU is fourth order (with a coefficient of $-1/6$).

For FEM-SUPG the asymptotic group speed representation is

$$\frac{\tilde{v}_g}{c} \sim 1 + \frac{3\beta}{2\mathbf{P}_e}(k\Delta x)^2 + \frac{15\beta - 180\beta^2 + 2\mathbf{P}_e(15\beta^2-1)}{72\mathbf{P}_e}(k\Delta x)^4 \tag{37}$$

For β_{opt} and infinite $\mathbf{P}_e$, the group speed is sixth-order accurate—similar to the phase speed.

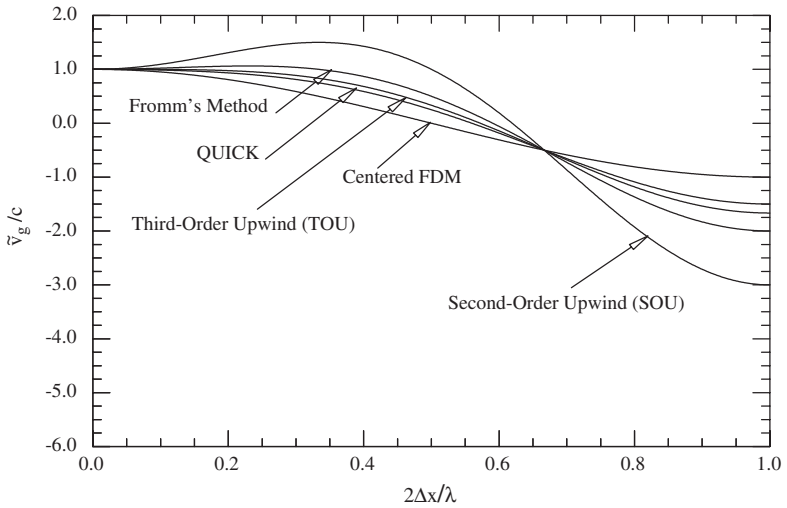

Figure 15. Non-dimensional group speed for a variety of finite-difference (node-centered finite-volume) methods.

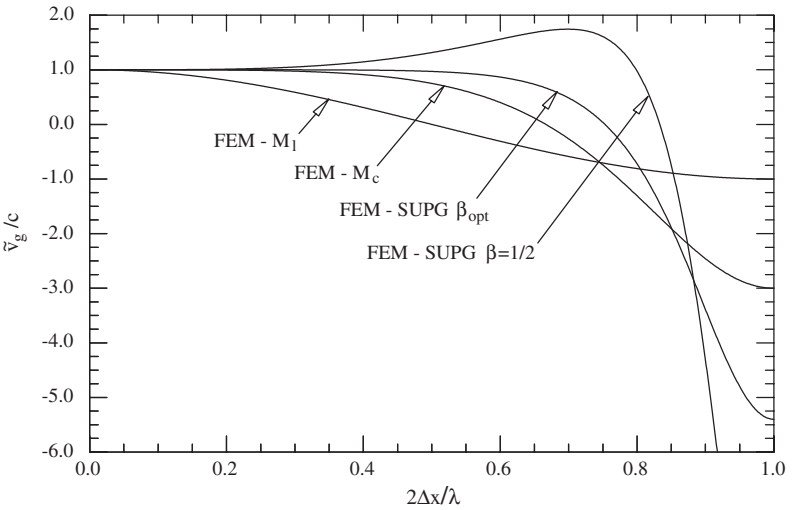

Figure 16. Non-dimensional group speed for finite element method using a consistent mass matrix (FEM-$\mathbf{M}_c$), lumped mass (FEM-$\mathbf{M}_l$), consistent mass matrix and SUPG (FEM-SUPG) with β_{opt} and $\beta = \frac{1}{2}$.

For $\beta = 0$, the asymptotic representation for FEM is recovered,

$$\frac{\tilde{v}_g}{c} \sim 1 - \frac{1}{36}(k\Delta x)^4 \tag{38}$$

which is fourth-order accurate.

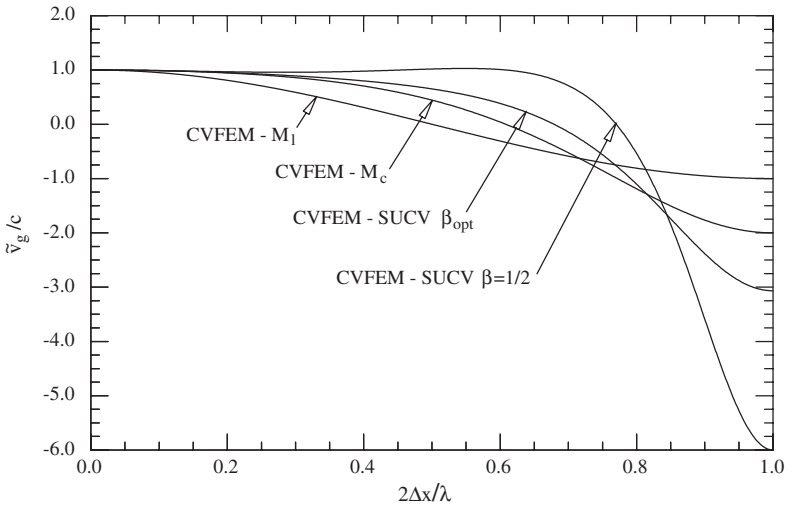

Figure 17. Non-dimensional group speed for control-volume finite element method using a consistent mass matrix (CVFEM-$\mathbf{M}_c$), lumped mass (CVFEM-$\mathbf{M}_l$), consistent mass matrix and SUCV (CVFEM-SUCV) with β_{opt} and $\beta = \frac{1}{2}$.

For SUCV the asymptotic representation is

$$\frac{\tilde{v}_g}{c} \sim 1 + \left(\frac{3\beta}{2\mathbf{P}_e} - \frac{1}{8}\right)(k\Delta x)^2 + \left(\frac{-7}{192} + \frac{5\beta^2}{8} - \frac{5\beta^2}{2\mathbf{P}_e}\right)(k\Delta x)^4 \tag{39}$$

For $\beta = 0$ the asymptotic representation of group speed for CVFEM is recovered,

$$\frac{\tilde{v}_g}{c} \sim 1 - \frac{1}{8}(k\Delta x)^2 - \frac{7}{192}(k\Delta x)^4 \tag{40}$$

Both CVFEM and CVFEM-SUCV are second-order accurate in the group speed.

The resolution requirements for a 5 and 1% error in group speed are shown with the asymptotic truncation error estimates in Table V. The best group speed accuracy for the least grid resolution is provided by FEM-SUPG with β_{opt} while the worst case is the second-order upwind method which, despite its second-order accuracy, requires more resolution than the first-order upwind method. Again, the CVFEM method exhibits reasonable resolution requirements for a 5% error in the group. However, for a 1% error, the resolution requirements increase significantly due to lagging group speed in the midrange of the discrete spectrum. For CVFEM-SUCV with $\beta = \frac{1}{2}$, the resolution requirements are about a factor of 4 times higher than for the FEM-SUPG method with the optimal stabilization parameter—a factor of 16 in two dimensions for equivalent error.

3.3. Discrete diffusivity

Attention is now turned to the behaviour of the discrete, wavelength-dependent diffusivity. The process of discretization introduces a wavelength dependence into the discrete thermal

Table V. Asymptotic estimates of truncation error and resolution requirements based on the group error for pure advection.

Method	Asymptotic T.E.	$\lambda/\Delta x$ for 5% Error	$\lambda/\Delta x$ for 1% Error
FOU	$O(\Delta x^2)$	19.7	44.4
SOU	$O(\Delta x^2)$	27.7	62.7
TOU	$O(\Delta x^4)$	8.29	12.6
QUICK	$O(\Delta x^2)$	11.2	22.9
Fromm's	$O(\Delta x^2)$	11.8	30.8
FEM-$\mathbf{M}_c$	$O(\Delta x^4)$	5.70	8.31
FEM-$\mathbf{M}_l$	$O(\Delta x^2)$	19.7	44.4
FEM-SUPG β_{opt}	$O(\Delta x^6)$	3.75	4.62
FEM-SUPG $\beta = \frac{1}{2}$	$O(\Delta x^4)$	6.70	10.3
CVFEM-$\mathbf{M}_c$	$O(\Delta x^2)$	10.4	22.5
CVFEM-$\mathbf{M}_l$	$O(\Delta x^2)$	19.7	44.4
CVFEM-SUCV β_{opt}	$O(\Delta x^2)$	9.88	22.2
CVFEM-SUCV $\beta = \frac{1}{2}$	$O(\Delta x^2)$	3.13	21.3

Note that the SUPG and SUCV results are presented only for a consistent mass matrix $\mathbf{M}_c$.

Table VI. Formulae for one-dimensional discrete diffusivity.

Method	Discrete diffusivity $(\tilde{\alpha}/\alpha)$
FDM/FVM	$2[1-\cos(k\Delta x)]/(k\Delta x)^2$
FEM/CVFEM	$\dfrac{2\mathscr{M}(k\Delta x)(1-\cos(k\Delta x))}{(k\Delta x)^2[\mathscr{M}^2(k\Delta x)+\beta^2\sin^2(k\Delta x)]}$

diffusivity even when a constant thermal diffusivity is prescribed for the continuum. The wavelength dependent behaviour of the discrete diffusivity indicates that individual modes that comprise a temperature profile will diffuse at different rates. The degree to which the rate of diffusion varies with wavelength is a function of the method chosen.

The formulae for the non-dimensional discrete diffusivity are presented in Table VI. All of the finite difference and finite volume methods use second-order centered approximations for the diffusion operator and yield identical discrete diffusivities as indicated by the single FDM/FVM entry in Table VI. The FEM/CVFEM ($\beta = 0$) with lumped mass matrix ($\mathscr{M}(k\Delta x) = 1$) also revert to the FDM/FVM formula.

The non-dimensional discrete diffusivity for the FEM, CVFEM (and FDM) methods are presented in Figure 18, and the results for FEM-SUPG and CVFEM-SUCV are presented in Figure 19. Here, we present the FEM-SUPG and CVFEM-SUCV results for the case when $\mathbf{P}_e > 3$ with a fixed stabilization parameter β. For $\mathbf{P}_e \leqslant 3$, the stabilization would presumably not be necessary. The ideal non-dimensional discrete diffusivity would be unity for the entire discrete wavelength spectrum. Thus, the deviation of the non-dimensional discrete diffusivity $\tilde{\alpha}/\alpha$ from unity may be interpreted as an error in discrete diffusivity relative to the continuum value of the diffusivity.

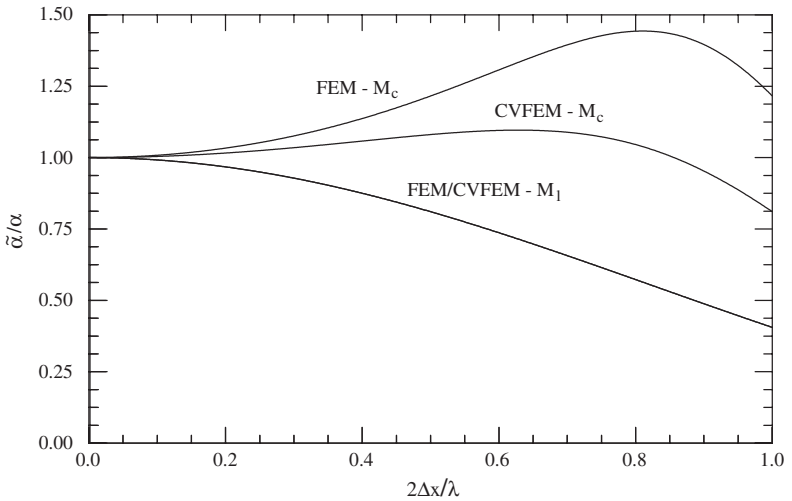

Figure 18. Non-dimensional discrete diffusivity for Galerkin finite element (FEM) and control-volume finite element methods (CVFEM).

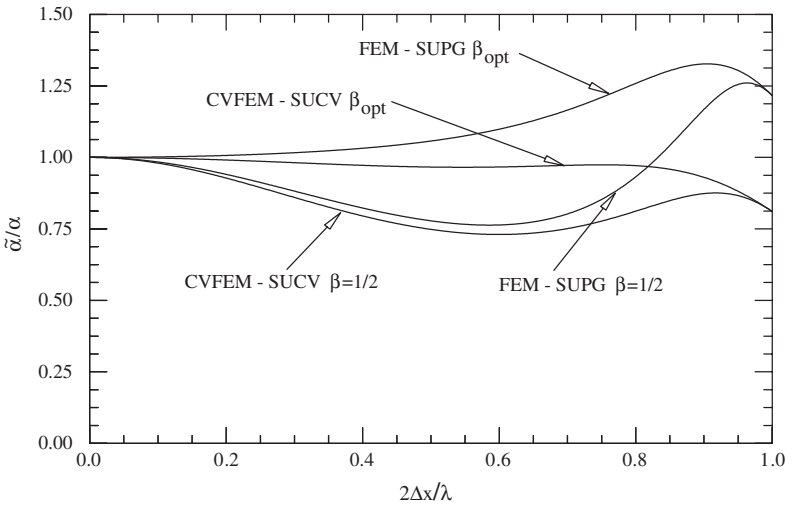

Figure 19. Non-dimensional discrete diffusivity for FEM with SUPG and CVFEM with SUCV.

The consistent mass FEM method (FEM-$\mathbf{M}_c$) exhibits an over-diffusive nature over the entire discrete spectrum, and the consistent mass CVFEM method (CVFEM-$\mathbf{M}_c$) is over-diffusive in the mid-range of the discrete spectrum. In contrast, the process of mass lumping yields discrete diffusivities for FEM and CVFEM that are under-diffusive for all discrete wavelengths. The FEM-SUPG and CVFEM-SUCV methods exhibit a sensitivity to the magnitude of the stabilization parameter, β. This demonstrates that a phase-error minimizing optimal value of the stabilization parameter for pure advection is not an optimal choice for thermal diffusion.

Table VII. Asymptotic estimates of truncation error and resolution requirements based on the discrete diffusivity for thermal diffusion.

Method	Asymptotic T.E.	$\lambda/\Delta x$ for 5% Error	$\lambda/\Delta x$ for 1% Error
FDM-Centered	$O(\Delta x^2)$	8.03	18.1
FEM-$\mathbf{M}_l$	$O(\Delta x^2)$	8.03	18.1
CVFEM-$\mathbf{M}_l$	$O(\Delta x^2)$	8.03	18.1
FEM-$\mathbf{M}_c$	$O(\Delta x^2)$	8.19	18.2
FEM-SUPG (β_{opt})	$O(\Delta x^2)$	4.20	8.37
FEM-SUPG ($\beta = \frac{1}{2}$)	$O(\Delta x^2)$	11.0	25.5
CVFEM-$\mathbf{M}_c$	$O(\Delta x^2)$	5.45	12.8
CVFEM-SUCV (β_{opt})	$O(\Delta x^2)$	2.30	9.52
CVFEM-SUCV ($\beta = \frac{1}{2}$)	$O(\Delta x^2)$	12.3	28.4

The finite volume schemes considered all share a common second-order centered discretization representation of the diffusion term in Equation (1) with an $O(\Delta x^2)$ truncation error as shown in Table VII. In one dimension, the lumped-mass FEM, lumped-mass CVFEM, and node-centered finite volume schemes all yield equivalent discrete diffusivities (Figure 18). Thus, the discrete diffusivity for FOU, SOU, TOU, etc. will be the same as the lumped mass result of Figure 18. Similarly, the node-centered finite volume scheme that introduces a consistent mass matrix (CD-$\mathbf{M}_c$) yields a discrete diffusivity that is identical to the FEM method with a consistent mass in one dimension. Note that the consistent mass CVFEM and CVFEM-SUCV (with β_{opt}) schemes yield the least error over the spectrum of dimensionless wave number (see Figures 18 and 19). While the SUPG and SUCV variants show favorable truncation error in discrete diffusivity, their use in a diffusion-dominated problem will add unwanted (and unnecessary) artifical diffusion (see Figure 21).

3.3.1. Asymptotic truncation error and resolution estimates. The asymptotic truncation error estimates for discrete diffusivity are summarized in Table VII. The mass-lumped FVM (or FDM) methods considered all share the same central difference approximation for the diffusion, resulting in the following asymptotic representation of discrete diffusivity

$$\frac{\tilde{\alpha}}{\alpha} \sim 1 - \frac{1}{12}(k\Delta x)^2 + \frac{1}{360}(k\Delta x)^4 \tag{41}$$

For FEM-SUPG (and FEM when $\beta = 0$), the asymptotic formula for the discrete diffusivity is

$$\frac{\tilde{\alpha}}{\alpha} \sim 1 - \left(\beta^2 - \frac{1}{12}\right)(k\Delta x)^2 + \left(\beta^4 - \frac{1}{12}\beta^2 + \frac{1}{360}\right)(k\Delta x)^4 \tag{42}$$

For CVFEM-SUCV (and CVFEM when $\beta = 0$), the asymptotic form of the discrete diffusivity is

$$\frac{\tilde{\alpha}}{\alpha} \sim 1 - \left(\beta^2 - \frac{1}{24}\right)(k\Delta x)^2 + \left(\beta^4 + \frac{1}{24}\beta^2 - \frac{7}{2880}\right)(k\Delta x)^4 \tag{43}$$

All of the finite element based methods are second-order for discrete diffusivity.

Table VIII. Formulae for one-dimensional artificial diffusivity.

Method	Artificial diffusivity $((\mathbf{P}_e^{\text{art}})^{-1} = 2\alpha_{\text{art}}/c\Delta x)$
FOU	$2[1-\cos(k\Delta x)]/(k\Delta x)^2$
SOU	$[3+\cos(2k\Delta x)-4\cos(k\Delta x)]/(k\Delta x)^2$
TOU	$[3+\cos(2k\Delta x)-4\cos(k\Delta x)]/3(k\Delta x)^2$
QUICK	$[3+\cos(2k\Delta x)-4\cos(k\Delta x)]/4(k\Delta x)^2$
Fromm's	$[3+\cos(2k\Delta x)-4\cos(k\Delta x)]/2(k\Delta x)^2$
SUPG/SUCV	$\dfrac{4\beta[\mathscr{M}(k\Delta x)(1-\cos(k\Delta x))-\sin^2(k\Delta x)/2]}{(k\Delta x)^2[\mathscr{M}^2(k\Delta x)+\beta^2\sin^2(k\Delta x)]}$

Finally, use of a lumped mass matrix (lumping the original mass matrix only) with FEM-SUPG or CVFEM-SUCV stabilization yields the following discrete diffusivity

$$\frac{\tilde{\alpha}}{\alpha} \sim 1 - \left(\beta^2 + \frac{1}{12}\right)(k\Delta x)^2 + \left(\beta^4 + \frac{5}{12}\beta^2 + \frac{1}{360}\right)(k\Delta x)^4 \tag{44}$$

which is identical to the discrete diffusivity for the centered difference method for $\beta = 0$.

The resolution requirements for a 5 and 1% error in discrete diffusivity are shown with the asymptotic truncation error estimates in Table VII. The best diffusivity accuracy for the least grid resolution is provided by FEM-SUPG (in term of the 1% error) with β_{opt}. The worst accuracy is obtained with the $\beta = \frac{1}{2}$ CVFEM-SUCV formulation with more than 28 grid points required per wavelength to yield a discrete diffusivity error of 1%. Nearly as bad is the FEM-SUPG, $\beta = \frac{1}{2}$ formulation.

3.4. *Artificial diffusivity*

Artificial diffusion can be added to a method either explicitly, e.g., via an explicit second- or fourth-order operator, or it can be a by-product of an upwind advective discretization (e.g. first-order upwinding). In general, artificial diffusion is not a desirable feature of a method, but it can be useful for removing unwanted numerical artifacts such as high frequency dispersion errors in convection-dominated problems. For hyperbolic conservation laws, i.e. pure advection in the context of this work, a 'properly tuned' artificial viscosity can be used to select the physically correct weak solution when non-smooth data is present.

The formulae for dimensionless artificial diffusion as a function of dimensionless wave number are shown in Table VIII for all the methods considered here.¶ In our opinion, an ideal artificial diffusivity should only be active in the high-frequency, short-wavelength portion of the discrete spectrum, near the Nyquist grid limit for example, and should be negligible otherwise. In this respect, Figure 20, which shows artificial diffusion for the FDM methods, illustrates the well-known problem with the first-order-upwind method. It behaves in the opposite manner to the ideal, maximizing the artificial diffusion as the grid is refined ($k\Delta x \to 0$). The higher order finite difference methods approximate the desired spectral behaviour, although they produce rather large amounts of artificial diffusion even in the mid-range frequencies

¶A factor of 1/2 is missing in the $\sin^2 k\Delta x$ term in the numerator of the artificial diffusion formula given in Reference [8] for FEM (see Equations (2.6)–(78)).

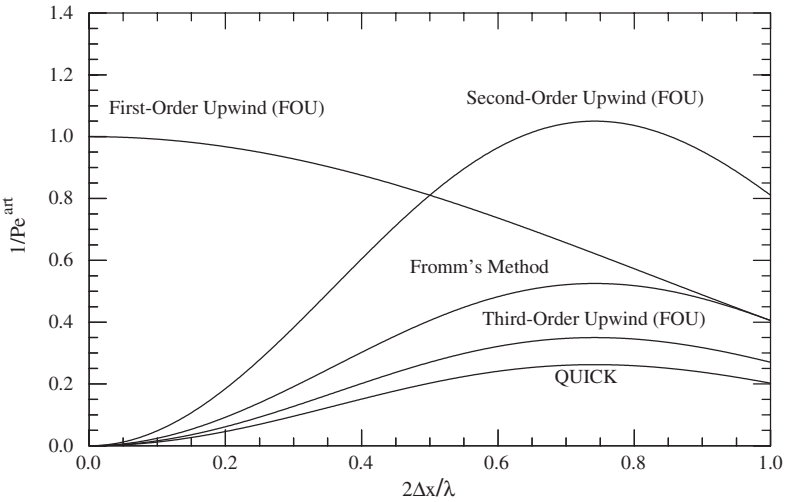

Figure 20. Non-dimensional artificial diffusivity for a variety of finite difference (node-centered finite-volume) methods.

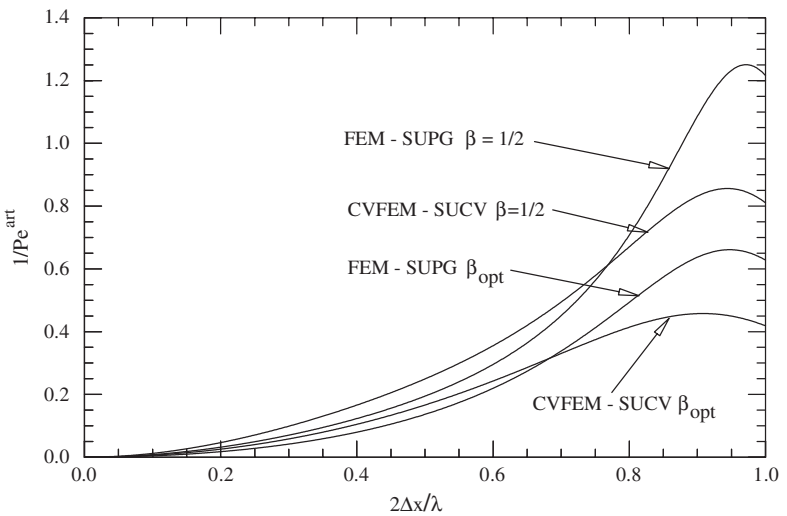

Figure 21. Non-dimensional artificial diffusivity for FEM-SUPG and CVFEM-SUCV.

when compared to the FEM-based methods shown in Figure 21. These methods come closest to the ideal spectral behaviour, with artificial diffusion remaining small (relative to its value at the Nyquist limit) until $2\Delta x/\lambda > 0.7$ permitting the signals with 'good' phase behaviour to survive the side-effects of the artificial diffusivity. The centered methods, i.e. FEM and CVFEM, do not introduce artificial diffusion and hence do not appear in these figures.

3.4.1. Asymptotic truncation error estimates. The order of truncation error in the artificial diffusivity for FOU is $O(1)$ while all of the other methods are $O(\Delta x^2)$. The order of truncation error indicates how quickly the artificial diffusivity approaches zero as a function of the non-dimensional wave number.

The non-dimensional artificial diffusivity may be written as

$$\frac{1}{\mathbf{P}_e^{\text{art}}} = \frac{2\alpha_{\text{art}}}{c\Delta x} \tag{45}$$

The asymptotic representation of the dimensionless artificial diffusivity for first-order upwind (FOU) is identical to the dimensionless discrete diffusivity in Equation (41),

$$\frac{1}{\mathbf{P}_e^{\text{art}}} \sim 1 - \frac{1}{12}(k\Delta x)^2 + \frac{1}{360}(k\Delta x)^4 \tag{46}$$

However, here the constant (unity) leading term in the asymptotic expansion indicates that the non-dimensional artificial viscosity ($1/\mathbf{P}_e^{\text{art}}$) approaches a constant quantity independent of $k\Delta x$. As demonstrated by the artificial viscosity results for FOU in Figure 20, $1/\mathbf{P}_e^{\text{art}} \to 1$ in the limit as $\Delta x \to 0$. It is important to note, however, that $\alpha_{\text{art}} \to 0$ as $\Delta x \to 0$ (see Equation (45)) so that first-order upwind is a consistent approximation to the pure advection problem.

The asymptotic expansion for SOU, Fromm, TOU and QUICK is

$$\frac{1}{\mathbf{P}_e^{\text{art}}} \sim \frac{1}{n}\left(\frac{1}{2}(k\Delta x)^2 - \frac{1}{12}(k\Delta x)^4 + \frac{1}{160}(k\Delta x)^6\right) \tag{47}$$

for $n = 1, 2, 3$ and 4, respectively. In contrast to FOU, these methods are all second order. Recall that the central difference scheme, FEM and CVFEM do not introduce any artificial diffusion. The asymptotic form for FEM-SUPG is

$$\frac{1}{\mathbf{P}_e^{\text{art}}} \sim 4\beta\left[\frac{(k\Delta x)^2}{24} + \frac{1}{144}(1 - 6\beta^2)(k\Delta x)^4 + O((k\Delta x)^6)\right] \tag{48}$$

Using the optimal value of $\beta(= 1/\sqrt{15})$, the formula becomes,

$$\frac{1}{\mathbf{P}_e^{\text{art}}} = \frac{1}{\sqrt{15}}\left[\frac{(k\Delta x)^2}{6} + \frac{(k\Delta x)^4}{60}\right] \tag{49}$$

For CVFEM-SUCV, the asymptotic form is

$$\frac{1}{\mathbf{P}_e^{\text{art}}} \sim 4\beta\left[\frac{(k\Delta x)^2}{16} + \frac{1}{192}(1 - 12\beta^2)(k\Delta x)^4 + O((k\Delta x)^6)\right] \tag{50}$$

Using $\beta = \frac{1}{2}$, which is near-optimal for dispersion, the formula becomes

$$\frac{1}{\mathbf{P}_e^{\text{art}}} = \frac{(k\Delta x)^2}{8} - \frac{(k\Delta x)^4}{48} \tag{51}$$

Thus, even though they are both second order, FEM-SUPG has the smaller leading coefficient; this is reflected in Figure 21.

Finally, if the mass matrix is lumped in either of SUPG or SUCV prior to applying the stabilization schemes, we get

$$\frac{1}{\mathbf{P}_e^{\text{art}}} \sim \frac{\beta}{2}\left[(k\Delta x)^2 - \left(\frac{1}{6}+\beta^2\right)(k\Delta x)^4 + O((k\Delta x)^6)\right] \tag{52}$$

3.5. *Effects of artificial diffusivity*

The results presented so far indicate that there is an interplay between the artificial diffusivity, phase and group errors, and discrete diffusivity. While, it is difficult to identify an 'ideal' artificial diffusivity, in our opinion, one that is active only in the high-frequency portion of the discrete spectrum is, at a minimum, desirable. We can gain some additional insight into the effects of the artificial diffusivity on the discrete solution by considering its effect on the time rate of change in the quadratic temperature, QT,

$$\frac{\mathrm{d}}{\mathrm{d}t}(QT) = \frac{1}{2}\frac{\mathrm{d}}{\mathrm{d}t}\int_\Omega \overline{T}T\,\mathrm{d}\Omega = \frac{\mathrm{d}}{\mathrm{d}t}\left(\frac{1}{2}\overline{T}^T\mathbf{M}_{\text{sym}}T\right) \tag{53}$$

where

$$\overline{T}_{m,n} = A\exp[-k^2\alpha_{\text{art}}t]\exp[-\imath k(m\Delta x\cos\theta + n\Delta y\sin\theta) + \imath\tilde{\omega}t] \tag{54}$$

is the complex conjugate of T and $\mathbf{M}_{\text{sym}}$ is the symmetric part of the mass matrix.

Remark
The quadratic temperature is a reasonable quantity to consider because it provides a 'natural' metric for quantifying the effects of artificial diffusivity. It is well-known that, for the advection–diffusion equation, methods that conserve the quadratic temperature generate stable ODEs—an important feature for long-time integration. In addition, it was also demonstrated by Lee *et al.* that conservation of T^2 can be more important than other forms of conservation where stability is concerned [40].

We can show that the quadratic temperature is impacted by the symmetric and skew-symmetric parts of the advective and mass operators respectively (note that this is trivial if T is only real) by considering the pure advection problem, i.e. no physical diffusivity,

$$\mathbf{M}_{\text{sym}}\dot{T} + \mathbf{M}_{\text{skew}}\dot{T} + \mathbf{A}_{\text{skew}}(c)T + \mathbf{A}_{\text{sym}}(c)T = 0 \tag{55}$$

First, as $\overline{T}$ and T are both solutions to the semi-discrete problem, we have

$$\overline{T}^{\mathrm{T}}\mathbf{M}_{\text{sym}}\dot{T} = -\overline{T}^{\mathrm{T}}\mathbf{M}_{\text{skew}}\dot{T} - \overline{T}^{\mathrm{T}}\mathbf{A}_{\text{skew}}(c)T - \overline{T}^{\mathrm{T}}\mathbf{A}_{\text{sym}}(c)T \tag{56}$$

and

$$T^{\mathrm{T}}\mathbf{M}_{\text{sym}}\overline{T} = -T^{\mathrm{T}}\mathbf{M}_{\text{skew}}\dot{\overline{T}} - T^{\mathrm{T}}\mathbf{A}_{\text{skew}}(c)\overline{T} - T^{\mathrm{T}}\mathbf{A}_{\text{sym}}(c)\overline{T} \tag{57}$$

where the semi-discrete equation for T ($\overline{T}$) has been pre-multiplied by $\overline{T}^{\mathrm{T}}$ (T^{T}). Further, the mass matrix has been separated into skew-symmetric, $\mathbf{M}_{\text{skew}}$, and symmetric, $\mathbf{M}_{\text{sym}}$, parts

in order to address the streamline-upwind finite element and control-volume finite element methods. Noting that

$$\frac{\mathrm{d}}{\mathrm{d}t}(QT)=\frac{\mathrm{d}}{\mathrm{d}t}\left(\frac{1}{2}\,\overline{T}^{\mathrm{T}}\mathbf{M}_{\mathrm{sym}}\overline{T}\right)=\frac{1}{2}\,\overline{T}^{\mathrm{T}}\mathbf{M}_{\mathrm{sym}}\dot{T}+\frac{1}{2}\,T^{\mathrm{T}}\mathbf{M}_{\mathrm{sym}}\dot{\overline{T}} \tag{58}$$

and substituting from Equations (56) and (57) yields,

$$\frac{\mathrm{d}}{\mathrm{d}t}\,(QT)=-\frac{1}{2}\,\overline{T}^{\mathrm{T}}\mathbf{M}_{\mathrm{skew}}\dot{T}-\frac{1}{2}\,T^{\mathrm{T}}\mathbf{M}_{\mathrm{skew}}\dot{\overline{T}}-\overline{T}^{\mathrm{T}}\mathbf{A}_{\mathrm{sym}}T \tag{59}$$

where $\overline{T}^{\mathrm{T}}\mathbf{B}_{\mathrm{sym}}T=T^{\mathrm{T}}\mathbf{B}_{\mathrm{sym}}\overline{T}$ and $\overline{T}^{\mathrm{T}}\mathbf{B}_{\mathrm{skew}}T=-T^{\mathrm{T}}\mathbf{B}_{\mathrm{skew}}\overline{T}$ are employed ($\mathbf{B}$ is any square matrix). Clearly, the quadratic temperature involves a complex interplay between artificial diffusivity (as it impacts T and $\overline{T}$), the symmetric part of the advection operator and the skew-symmetric part of the mass matrix.

In order to understand the effect of the artificial diffusivity on the quadratic temperature, we consider an advective time-scale $\tau=\Delta x/c$ and integrate Equation (53) with respect to the time to obtain the incremental change in QT over τ,

$$QT_{t+\tau}-QT_t=\int_t^{t+\tau}\frac{\mathrm{d}}{\mathrm{d}t}\left(\frac{1}{2}\,\overline{T}^{\mathrm{T}}\mathbf{M}_{\mathrm{sym}}T\right)\mathrm{d}t \tag{60}$$

Substituting the general solution and its complex conjugate yields the quadratic temperature at an arbitrary time, t,

$$QT_t=A^2\exp^2[-k^2\alpha_{\mathrm{art}}t]\times\sum_{m=1}^{NP}\sum_{n=1}^{NP}\left\{\exp[-\imath k(x_{m,n}\cos\theta+y_{m,n}\sin\theta)]M^{\mathrm{sym}}_{m,n}\right\} \tag{61}$$

where $\mathbf{M}^{\mathrm{sym}}_{m,n}$ is the mth row, nth column entry in $\mathbf{M}_{\mathrm{sym}}$ and NP is the number of rows/columns. Note that QT is generally a function both of time, t, and wave number k.

In order to permit direct comparison between methods, we use the quadratic temperature at time t to construct a non-dimensional quadratic temperature increment over the advective time-scale τ as

$$\Delta QT=\frac{QT_{t+\tau}-QT_t}{QT_t} \tag{62}$$

In terms of this definition, it is clear that a method characterized by constant QT (i.e. no damping of quadratic temperature) produces $\Delta QT=0$ while $\Delta QT=-1$ indicates a method with complete damping of the associated waveform in one advective time scale τ.

After substitution into Equation (62) and cancellation of terms, the non-dimensional quadratic temperature increment may be written as,

$$\Delta QT=\exp^2[-k^2\Delta x^2/(2\mathbf{P}^{\mathrm{art}}_e)] \tag{63}$$

where it is clear the ΔQT is dependent on wave number and grid spacing (as is $\mathbf{P}^{\mathrm{art}}_e$). Finally, note that Equation (63) is a general statement of the quadratic temperature increment for any

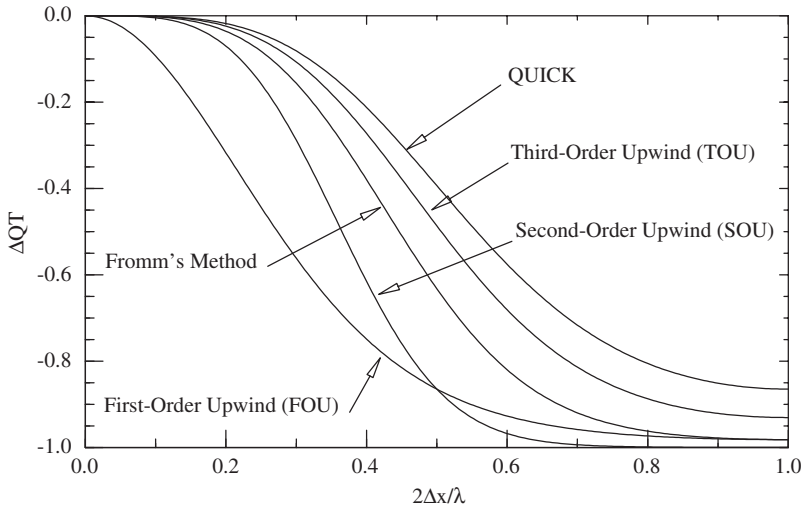

Figure 22. Non-dimensional change in incremental quadratic temperature, ΔQT, for a variety of finite difference (node-centered finite-volume) methods.

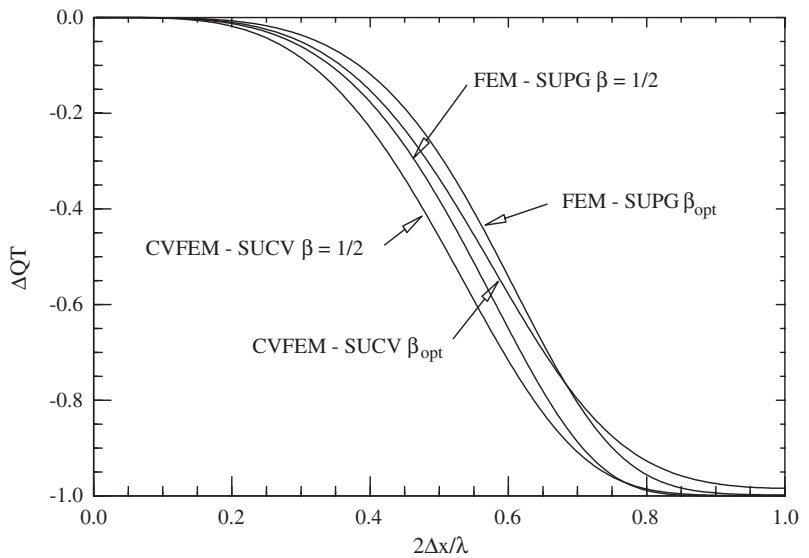

Figure 23. Non-dimensional change in incremental quadratic temperature, ΔQT, for FEM-SUPG and CVFEM-SUCV with $\beta = \beta_{\text{opt}}$ and $\frac{1}{2}$.

of the methods considered in this document. Indeed, the only method-dependent part occurs in the artificial diffusivity contained in $\mathbf{P}_e^{\text{art}}$.

As noted above, an ideal artificial diffusivity (and hence energy damping) should only be active in the high-frequency, short-wavelength portion of the discrete spectrum. In this respect, Figure 22, which shows ΔQT for the FDM methods, illustrates that this general

behaviour is respected. The higher order SOU and Fromm's methods approximate the desired spectral behaviour, although they produce rather large amounts of damping even in the mid-range frequencies when compared to the FEM-based methods shown in Figure 23. Conversely, QUICK and TOU both perform quite well in the low frequency range, but do not completely damp high-frequency signals ($2\Delta x/\lambda = 1$) over the advective time-scale.

In contrast, the FEM/CVFEM schemes appear to be nearly ideal (relative to the other methods presented here), with modest damping at low-frequencies, long-wavelengths, complete damping of the high-frequency, short-wavelength signals and a smooth transition in the mid-frequency range. Again, an assessment of the 'best' damping characteristics depends on the complex interplay between artificial diffusivity, phase and group speeds.

This concludes the discussion of the one-dimensional results. In Part 2 of this paper, the two-dimensional results are presented along with a summary of the one- and two-dimensional results and concluding remarks.

APPENDIX A

The semi-discrete equations for each of the methods considered in this work are presented here with the advection operators decomposed into symmetric and skew-symmetric components where appropriate. Each of the semi-discrete equations is presented in a stencil form based on the grid layout shown in Figure 1.

The generic form for the semi-discrete equations is

$$\mathbf{M}\dot{T} + \mathbf{A}_x(u)T + \mathbf{A}_y(v)T + \mathbf{K}T = 0 \tag{A1}$$

For each operator in the semi-discrete equation, the 'stencil' entries multiply their respective (m,n) field variables, e.g., for a generic operator A,

$$A = \begin{array}{|ccccc|} \hline (m-2,n+2) & (m-1,n+2) & (m,n+2) & (m+1,n+2) & (m+2,n+2) \\ (m-2,n+1) & (m-1,n+1) & (m,n+1) & (m+1,n+1) & (m+2,n+1) \\ (m-2,n) & (m-1,n) & (m,n) & (m+1,n) & (m+2,n) \\ (m-2,n-1) & (m-1,n-1) & (m,n-1) & (m+1,n-1) & (m+2,n-1) \\ (m-2,n-2) & (m-1,n-2) & (m,n-2) & (m+1,n-2) & (m+2,n-2) \\ \hline \end{array} \tag{A2}$$

A.1. First-order upwind (FOU)

$$\Delta x\Delta y \begin{array}{|ccc|} \hline 0 & 0 & 0 \\ 0 & 1 & 0 \\ 0 & 0 & 0 \\ \hline \end{array} \dot{T} + u\Delta y \begin{array}{|ccc|} \hline 0 & 0 & 0 \\ -1 & 1 & 0 \\ 0 & 0 & 0 \\ \hline \end{array} T + v\Delta x \begin{array}{|ccc|} \hline 0 & 0 & 0 \\ 0 & 1 & 0 \\ 0 & -1 & 0 \\ \hline \end{array} T$$

$$-\alpha \begin{bmatrix} 0 & \dfrac{\Delta x}{\Delta y} & 0 \\ \dfrac{\Delta y}{\Delta x} & -2\left(\dfrac{\Delta y}{\Delta x}+\dfrac{\Delta x}{\Delta y}\right) & \dfrac{\Delta y}{\Delta x} \\ 0 & \dfrac{\Delta x}{\Delta y} & 0 \end{bmatrix} T = 0 \tag{A3}$$

This equation represents the stencil for the FOU method in the form presented in Equation (A2). The first term represents the discrete mass matrix operator, the next two terms are the x- and y-components of the advection operator, and the last term is the stencil for the discrete representation of diffusion. It is illustrative to decompose the advection operator into symmetric and skew-symmetric operators; the former represents the artificial diffusivity in the method. The symmetric and skew-symmetric portions of the first-order upwind advection operator are,

$$\mathbf{A}_x = u\Delta y \begin{bmatrix} 0 & 0 & 0 \\ -1/2 & 1 & -1/2 \\ 0 & 0 & 0 \end{bmatrix} + u\Delta y \begin{bmatrix} 0 & 0 & 0 \\ -1/2 & 0 & 1/2 \\ 0 & 0 & 0 \end{bmatrix} \tag{A4}$$

for the x-co-ordinate operator, and

$$\mathbf{A}_y = v\Delta x \begin{bmatrix} 0 & -1/2 & 0 \\ 0 & 1 & 0 \\ 0 & -1/2 & 0 \end{bmatrix} + v\Delta x \begin{bmatrix} 0 & 1/2 & 0 \\ 0 & 0 & 0 \\ 0 & -1/2 & 0 \end{bmatrix} \tag{A5}$$

for the y-coordinate operator. Clearly, the first stencil on the right-hand side of each component equation is the symmetric contribution, and if the two symmetric components are summed with the diffusion operator, the result is the classical expression for artificial diffusivity for the first-order upwind scheme, with the form $\alpha_{\text{art},x} \sim u\Delta x$ and $\alpha_{\text{art},y} \sim v\Delta y$.

A.2. Second-order central difference (CD)

$$\Delta x\Delta y \begin{bmatrix} 0 & 0 & 0 \\ 0 & 1 & 0 \\ 0 & 0 & 0 \end{bmatrix} \dot{T} + u\Delta y \begin{bmatrix} 0 & 0 & 0 \\ -1/2 & 0 & 1/2 \\ 0 & 0 & 0 \end{bmatrix} T + v\Delta x \begin{bmatrix} 0 & 1/2 & 0 \\ 0 & 0 & 0 \\ 0 & -1/2 & 0 \end{bmatrix} T$$

$$-\alpha \begin{bmatrix} 0 & \dfrac{\Delta x}{\Delta y} & 0 \\ \dfrac{\Delta y}{\Delta x} & -2\left(\dfrac{\Delta y}{\Delta x}+\dfrac{\Delta x}{\Delta y}\right) & \dfrac{\Delta y}{\Delta x} \\ 0 & \dfrac{\Delta x}{\Delta y} & 0 \end{bmatrix} T = 0 \tag{A6}$$

The components of the skew-symmetric advective operator are the second and third terms. There is no symmetric portion to this advective operator and hence no artificial diffusion in this method.

We also consider an *ad hoc* version of this scheme, referred to as a centered difference method with consistent mass (CD-$\mathbf{M}_c$), in which the lumped mass term in the foregoing equation is replaced with the consistent mass matrix from CVFEM:

$$\frac{\Delta x \Delta y}{64} \begin{bmatrix} 1 & 6 & 1 \\ 6 & 36 & 6 \\ 1 & 6 & 1 \end{bmatrix} \dot{T} \tag{A7}$$

This scheme is *ad hoc* because the spatial representation of the time derivative term is different from that for the advective and diffusive terms in order to arrive at this form.

A.3. Second-order upwind (SOU)

$$\Delta x \Delta y \begin{bmatrix} 0 & 0 & 0 \\ 0 & 1 & 0 \\ 0 & 0 & 0 \end{bmatrix} \dot{T} + \frac{u\Delta y}{2} \begin{bmatrix} 0 & 0 & 0 & 0 & 0 \\ 0 & 0 & 0 & 0 & 0 \\ 1 & -4 & 3 & 0 & 0 \\ 0 & 0 & 0 & 0 & 0 \\ 0 & 0 & 0 & 0 & 0 \end{bmatrix} T + \frac{v\Delta x}{2} \begin{bmatrix} 0 & 0 & 0 & 0 & 0 \\ 0 & 0 & 0 & 0 & 0 \\ 0 & 0 & 3 & 0 & 0 \\ 0 & 0 & -4 & 0 & 0 \\ 0 & 0 & 1 & 0 & 0 \end{bmatrix} T$$

$$-\alpha \mathbf{K_{CD}} T = 0 \tag{A8}$$

where $\mathbf{K_{CD}}$ denotes the 5-pt central difference stencil for the diffusion operator, given by the last operator in the FOU stencil, Equation (A3) above. The symmetric and skew-symmetric

portions of the second-order upwind advection operator are,

$$\mathbf{A}_x = \frac{u\Delta y}{2}\begin{bmatrix} 0 & 0 & 0 & 0 & 0 \\ 0 & 0 & 0 & 0 & 0 \\ 1/2 & -2 & 3 & -2 & 1/2 \\ 0 & 0 & 0 & 0 & 0 \\ 0 & 0 & 0 & 0 & 0 \end{bmatrix} + \frac{u\Delta y}{2}\begin{bmatrix} 0 & 0 & 0 & 0 & 0 \\ 0 & 0 & 0 & 0 & 0 \\ 1/2 & -2 & 0 & 2 & -1/2 \\ 0 & 0 & 0 & 0 & 0 \\ 0 & 0 & 0 & 0 & 0 \end{bmatrix} \tag{A9}$$

and

$$\mathbf{A}_y = \frac{v\Delta x}{2}\begin{bmatrix} 0 & 0 & 1/2 & 0 & 0 \\ 0 & 0 & -2 & 0 & 0 \\ 0 & 0 & 3 & 0 & 0 \\ 0 & 0 & -2 & 0 & 0 \\ 0 & 0 & 1/2 & 0 & 0 \end{bmatrix} + \frac{v\Delta x}{2}\begin{bmatrix} 0 & 0 & -1/2 & 0 & 0 \\ 0 & 0 & 2 & 0 & 0 \\ 0 & 0 & 0 & 0 & 0 \\ 0 & 0 & -2 & 0 & 0 \\ 0 & 0 & 1/2 & 0 & 0 \end{bmatrix} \tag{A10}$$

for the x- and y-components, respectively.

A.4. Third-order upwind (TOU)

$$\Delta x\Delta y \begin{bmatrix} 0 & 0 & 0 \\ 0 & 1 & 0 \\ 0 & 0 & 0 \end{bmatrix} \dot{T} + \frac{u\Delta y}{12}\begin{bmatrix} 0 & 0 & 0 & 0 & 0 \\ 0 & 0 & 0 & 0 & 0 \\ 2 & -12 & 6 & 4 & 0 \\ 0 & 0 & 0 & 0 & 0 \\ 0 & 0 & 0 & 0 & 0 \end{bmatrix} T + \frac{v\Delta x}{12}\begin{bmatrix} 0 & 0 & 0 & 0 & 0 \\ 0 & 0 & 4 & 0 & 0 \\ 0 & 0 & 6 & 0 & 0 \\ 0 & 0 & -12 & 0 & 0 \\ 0 & 0 & 2 & 0 & 0 \end{bmatrix} T$$

$$-\alpha\mathbf{K}_{\mathbf{CD}}T = 0 \tag{A11}$$

The symmetric and skew-symmetric portions of the third-order upwind-biased scheme are,

$$\mathbf{A}_x = \frac{u\Delta y}{12}\begin{bmatrix} 0 & 0 & 0 & 0 & 0 \\ 0 & 0 & 0 & 0 & 0 \\ 1 & -4 & 6 & -4 & 1 \\ 0 & 0 & 0 & 0 & 0 \\ 0 & 0 & 0 & 0 & 0 \end{bmatrix} + \frac{u\Delta y}{12}\begin{bmatrix} 0 & 0 & 0 & 0 & 0 \\ 0 & 0 & 0 & 0 & 0 \\ 1 & -8 & 0 & 8 & -1 \\ 0 & 0 & 0 & 0 & 0 \\ 0 & 0 & 0 & 0 & 0 \end{bmatrix} \tag{A12}$$

and

$$\mathbf{A}_y = \frac{v\Delta x}{12}\begin{bmatrix} 0 & 0 & 1 & 0 & 0 \\ 0 & 0 & -4 & 0 & 0 \\ 0 & 0 & 6 & 0 & 0 \\ 0 & 0 & -4 & 0 & 0 \\ 0 & 0 & 1 & 0 & 0 \end{bmatrix} + \frac{v\Delta x}{12}\begin{bmatrix} 0 & 0 & -1 & 0 & 0 \\ 0 & 0 & 8 & 0 & 0 \\ 0 & 0 & 0 & 0 & 0 \\ 0 & 0 & -8 & 0 & 0 \\ 0 & 0 & 1 & 0 & 0 \end{bmatrix} \tag{A13}$$

for the x- and y-components, respectively.

A.5. Fromm's method

$$\Delta x\Delta y \begin{bmatrix} 0 & 0 & 0 \\ 0 & 1 & 0 \\ 0 & 0 & 0 \end{bmatrix} \dot{T} + \frac{u\Delta y}{4}\begin{bmatrix} 0 & 0 & 0 & 0 & 0 \\ 0 & 0 & 0 & 0 & 0 \\ 1 & -5 & 3 & 1 & 0 \\ 0 & 0 & 0 & 0 & 0 \\ 0 & 0 & 0 & 0 & 0 \end{bmatrix} T + \frac{v\Delta x}{4}\begin{bmatrix} 0 & 0 & 0 & 0 & 0 \\ 0 & 0 & 1 & 0 & 0 \\ 0 & 0 & 3 & 0 & 0 \\ 0 & 0 & -5 & 0 & 0 \\ 0 & 0 & 1 & 0 & 0 \end{bmatrix} T$$
$$-\alpha \mathbf{K}_{\mathbf{CD}} T = 0 \tag{A14}$$

The symmetric and skew-symmetric portions of the advection operator in the Fromm upwind-biased scheme are,

$$\mathbf{A}_x = \frac{u\Delta y}{4}\begin{bmatrix} 0 & 0 & 0 & 0 & 0 \\ 0 & 0 & 0 & 0 & 0 \\ 1/2 & -2 & 3 & -2 & 1/2 \\ 0 & 0 & 0 & 0 & 0 \\ 0 & 0 & 0 & 0 & 0 \end{bmatrix} + \frac{u\Delta y}{4}\begin{bmatrix} 0 & 0 & 0 & 0 & 0 \\ 0 & 0 & 0 & 0 & 0 \\ 1/2 & -3 & 0 & 3 & -1/2 \\ 0 & 0 & 0 & 0 & 0 \\ 0 & 0 & 0 & 0 & 0 \end{bmatrix} \tag{A15}$$

and

$$\mathbf{A}_y = \frac{v\Delta x}{4}\begin{bmatrix} 0 & 0 & 1/2 & 0 & 0 \\ 0 & 0 & -2 & 0 & 0 \\ 0 & 0 & 3 & 0 & 0 \\ 0 & 0 & -2 & 0 & 0 \\ 0 & 0 & 1/2 & 0 & 0 \end{bmatrix} + \frac{c_y\Delta x}{4}\begin{bmatrix} 0 & 0 & -1/2 & 0 & 0 \\ 0 & 0 & 3 & 0 & 0 \\ 0 & 0 & 0 & 0 & 0 \\ 0 & 0 & -3 & 0 & 0 \\ 0 & 0 & 1/2 & 0 & 0 \end{bmatrix} \tag{A16}$$

for the x- and y-components, respectively.

A.6. Quick

$$\Delta x\Delta y \begin{bmatrix} 0 & 0 & 0 \\ 0 & 1 & 0 \\ 0 & 0 & 0 \end{bmatrix} \dot{T} + \frac{u\Delta y}{8} \begin{bmatrix} 0 & 0 & 0 & 0 & 0 \\ 0 & 0 & 0 & 0 & 0 \\ 1 & -7 & 3 & 3 & 0 \\ 0 & 0 & 0 & 0 & 0 \\ 0 & 0 & 0 & 0 & 0 \end{bmatrix} T + \frac{v\Delta x}{8} \begin{bmatrix} 0 & 0 & 0 & 0 & 0 \\ 0 & 0 & 3 & 0 & 0 \\ 0 & 0 & 3 & 0 & 0 \\ 0 & 0 & -7 & 0 & 0 \\ 0 & 0 & 1 & 0 & 0 \end{bmatrix} T$$

$$-\alpha \mathbf{K}_{\mathbf{CD}} T = 0 \tag{A17}$$

The symmetric and skew-symmetric portions of the advection operator in the QUICK scheme are

$$\mathbf{A}_x = \frac{u\Delta y}{8} \begin{bmatrix} 0 & 0 & 0 & 0 & 0 \\ 0 & 0 & 0 & 0 & 0 \\ 1/2 & -2 & 3 & -2 & 1/2 \\ 0 & 0 & 0 & 0 & 0 \\ 0 & 0 & 0 & 0 & 0 \end{bmatrix} + \frac{u\Delta y}{8} \begin{bmatrix} 0 & 0 & 0 & 0 & 0 \\ 0 & 0 & 0 & 0 & 0 \\ 1/2 & -5 & 0 & 5 & -1/2 \\ 0 & 0 & 0 & 0 & 0 \\ 0 & 0 & 0 & 0 & 0 \end{bmatrix} \tag{A18}$$

and

$$\mathbf{A}_y = \frac{v\Delta x}{8} \begin{bmatrix} 0 & 0 & 1/2 & 0 & 0 \\ 0 & 0 & -2 & 0 & 0 \\ 0 & 0 & 3 & 0 & 0 \\ 0 & 0 & -2 & 0 & 0 \\ 0 & 0 & 1/2 & 0 & 0 \end{bmatrix} + \frac{v\Delta x}{8} \begin{bmatrix} 0 & 0 & -1/2 & 0 & 0 \\ 0 & 0 & 5 & 0 & 0 \\ 0 & 0 & 0 & 0 & 0 \\ 0 & 0 & -5 & 0 & 0 \\ 0 & 0 & 1/2 & 0 & 0 \end{bmatrix} \tag{A19}$$

for the x- and y-components, respectively.

A.7. Node-centered finite volume with least-squares gradient reconstruction (LSR)

Two methods that result from applying an unweighted least squares gradient reconstruction scheme were introduced in Section 2.3. The stencil for the LSR(-1) ($\psi = 1$ and $\kappa = -1$)

is given by

$$\Delta x\Delta y \begin{bmatrix} 0 & 0 & 0 \\ 0 & 1 & 0 \\ 0 & 0 & 0 \end{bmatrix} \dot{\overline{T}} + \frac{u\Delta y}{6} \begin{bmatrix} 0 & 0 & 0 & 0 & 0 \\ 1 & -1 & -1 & 1 & 0 \\ 1 & -10 & 11 & -2 & 0 \\ 1 & -1 & -1 & 1 & 0 \\ 0 & 0 & 0 & 0 & 0 \end{bmatrix} \overline{T}$$

$$+ \frac{v\Delta x}{6} \begin{bmatrix} 0 & 0 & 0 & 0 & 0 \\ 0 & 1 & -2 & 1 & 0 \\ 0 & -1 & 11 & -1 & 0 \\ 0 & -1 & -10 & -1 & 0 \\ 0 & 1 & 1 & 1 & 0 \end{bmatrix} \overline{T}$$

$$-\alpha \mathbf{K}_{\mathbf{CD}} \overline{T} = 0 \tag{A20}$$

The symmetric and skew-symmetric portions of the LSR(-1) scheme are

$$\mathbf{A}_x = \frac{u\Delta y}{6} \begin{bmatrix} 0 & 0 & 0 & 0 & 0 \\ 1/2 & 0 & -1 & 0 & 1/2 \\ 1/2 & -6 & 11 & -6 & 1/2 \\ 1/2 & 0 & -1 & 0 & 1/2 \\ 0 & 0 & 0 & 0 & 0 \end{bmatrix} + \frac{u\Delta y}{6} \begin{bmatrix} 0 & 0 & 0 & 0 & 0 \\ 1/2 & -1 & 0 & 1 & -1/2 \\ 1/2 & -4 & 0 & 4 & -1/2 \\ 1/2 & -1 & 0 & 1 & -1/2 \\ 0 & 0 & 0 & 0 & 0 \end{bmatrix} \tag{A21}$$

and

$$\mathbf{A}_y = \frac{v\Delta x}{6} \begin{bmatrix} 0 & 1/2 & 1/2 & 1/2 & 0 \\ 0 & 0 & -6 & 0 & 0 \\ 0 & -1 & 11 & -1 & 0 \\ 0 & 0 & -6 & 0 & 0 \\ 0 & 1/2 & 1/2 & 1/2 & 0 \end{bmatrix} + \frac{v\Delta x}{6} \begin{bmatrix} 0 & -1/2 & -1/2 & -1/2 & 0 \\ 0 & 1 & 4 & 1 & 0 \\ 0 & 0 & 0 & 0 & 0 \\ 0 & -1 & -4 & -1 & 0 \\ 0 & 1/2 & 1/2 & 1/2 & 0 \end{bmatrix} \tag{A22}$$

The stencil for the LSR(0) ($\psi = 1$ and $\kappa = 0$) scheme is given by

$$\Delta x \Delta y \begin{bmatrix} 0 & 0 & 0 \\ 0 & 1 & 0 \\ 0 & 0 & 0 \end{bmatrix} \dot{\overline{T}} + \frac{u\Delta y}{12} \begin{bmatrix} 0 & 0 & 0 & 0 & 0 \\ 1 & -1 & -1 & 1 & 0 \\ 1 & -13 & 11 & 1 & 0 \\ 1 & -1 & -1 & 1 & 0 \\ 0 & 0 & 0 & 0 & 0 \end{bmatrix} \overline{T}$$

$$+ \frac{v\Delta x}{12} \begin{bmatrix} 0 & 0 & 0 & 0 & 0 \\ 0 & 1 & 1 & 1 & 0 \\ 0 & -1 & 11 & -1 & 0 \\ 0 & -1 & -13 & -1 & 0 \\ 0 & 1 & 1 & 1 & 0 \end{bmatrix} \overline{T}$$

$$-\alpha \mathbf{K_{CD}} \overline{T} = 0 \tag{A23}$$

The symmetric and skew-symmetric portions of the LSR(0) scheme are:

$$\mathbf{A}_x = \frac{u\Delta y}{12} \begin{bmatrix} 0 & 0 & 0 & 0 & 0 \\ 1/2 & 0 & -1 & 0 & 1/2 \\ 1/2 & -6 & 11 & -6 & 1/2 \\ 1/2 & 0 & -1 & 0 & 1/2 \\ 0 & 0 & 0 & 0 & 0 \end{bmatrix} + \frac{u\Delta y}{12} \begin{bmatrix} 0 & 0 & 0 & 0 & 0 \\ 1/2 & -1 & 0 & 1 & -1/2 \\ 1/2 & -7 & 0 & 7 & -1/2 \\ 1/2 & -1 & 0 & 1 & -1/2 \\ 0 & 0 & 0 & 0 & 0 \end{bmatrix} \tag{A24}$$

and

$$\mathbf{A}_y = \frac{v\Delta x}{12} \begin{bmatrix} 0 & 1/2 & 1/2 & 1/2 & 0 \\ 0 & 0 & -6 & 0 & 0 \\ 0 & -1 & 11 & -1 & 0 \\ 0 & 0 & -6 & 0 & 0 \\ 0 & 1/2 & 1/2 & 1/2 & 0 \end{bmatrix} + \frac{v\Delta x}{12} \begin{bmatrix} 0 & -1/2 & -1/2 & -1/2 & 0 \\ 0 & 1 & 7 & 1 & 0 \\ 0 & 0 & 0 & 0 & 0 \\ 0 & -1 & -7 & -1 & 0 \\ 0 & 1/2 & 1/2 & 1/2 & 0 \end{bmatrix} \tag{A25}$$

A.8. Galerkin finite element method (FEM)

The full stencil for the Galerkin finite element method reads

$$\frac{\Delta x\Delta y}{36}\begin{bmatrix}1&4&1\\4&16&4\\1&4&1\end{bmatrix}\dot{T}+\frac{u\Delta y}{12}\begin{bmatrix}-1&0&1\\-4&0&4\\-1&0&1\end{bmatrix}T+\frac{v\Delta x}{12}\begin{bmatrix}1&4&1\\0&0&0\\-1&-4&-1\end{bmatrix}T$$

$$=\frac{\alpha}{6}\begin{bmatrix}\dfrac{\Delta y}{\Delta x}+\dfrac{\Delta x}{\Delta y} & 4\dfrac{\Delta x}{\Delta y}-2\dfrac{\Delta y}{\Delta x} & \dfrac{\Delta y}{\Delta x}+\dfrac{\Delta x}{\Delta y}\\ 4\dfrac{\Delta y}{\Delta x}-2\dfrac{\Delta x}{\Delta y} & -8\left(\dfrac{\Delta y}{\Delta x}+\dfrac{\Delta x}{\Delta y}\right) & 4\dfrac{\Delta y}{\Delta x}-2\dfrac{\Delta x}{\Delta y}\\ \dfrac{\Delta y}{\Delta x}+\dfrac{\Delta x}{\Delta y} & 4\dfrac{\Delta x}{\Delta y}-2\dfrac{\Delta y}{\Delta x} & \dfrac{\Delta y}{\Delta x}+\dfrac{\Delta x}{\Delta y}\end{bmatrix}T \tag{A26}$$

The components of the skew-symmetric portion of the advective operator are the second and third terms; there is no symmetric portion to this operator.

A.9. Finite element method with SUPG (FEM-SUPG)

The stencil for the SUPG method contains a modified mass matrix and an artificial diffusion term,

$$\frac{\Delta x\Delta y}{36}\begin{bmatrix}1&4&1\\4&16&4\\1&4&1\end{bmatrix}\dot{T}+\tau\frac{u\Delta y}{12}\begin{bmatrix}1&0&-1\\4&0&-4\\1&0&-1\end{bmatrix}\dot{T}+\tau\frac{v\Delta x}{12}\begin{bmatrix}-1&-4&-1\\0&0&0\\1&4&1\end{bmatrix}\dot{T}$$

$$+\frac{u\Delta y}{12}\begin{bmatrix}-1&0&1\\-4&0&4\\-1&0&1\end{bmatrix}T+\frac{v\Delta x}{12}\begin{bmatrix}1&4&1\\0&0&0\\-1&-4&-1\end{bmatrix}T$$

$$-\frac{\tau}{6}\begin{bmatrix}u^2\dfrac{\Delta y}{\Delta x}-3uv+v^2\dfrac{\Delta x}{\Delta y} & 4v^2\dfrac{\Delta x}{\Delta y}-2u^2\dfrac{\Delta y}{\Delta x} & u^2\dfrac{\Delta y}{\Delta x}+3uv+v^2\dfrac{\Delta x}{\Delta y}\\ 4u^2\dfrac{\Delta y}{\Delta x}-2v^2\dfrac{\Delta x}{\Delta y} & -8\left(u^2\dfrac{\Delta y}{\Delta x}+v^2\dfrac{\Delta x}{\Delta y}\right) & 4u^2\dfrac{\Delta y}{\Delta x}-2v^2\dfrac{\Delta x}{\Delta y}\\ u^2\dfrac{\Delta y}{\Delta x}+3uv+v^2\dfrac{\Delta x}{\Delta y} & 4v^2\dfrac{\Delta x}{\Delta y}-2u^2\dfrac{\Delta y}{\Delta x} & u^2\dfrac{\Delta y}{\Delta x}-3uv+v^2\dfrac{\Delta x}{\Delta y}\end{bmatrix}T$$

$$= \frac{\alpha}{6}\begin{bmatrix} \frac{\Delta y}{\Delta x}+\frac{\Delta x}{\Delta y} & 4\frac{\Delta x}{\Delta y}-2\frac{\Delta y}{\Delta x} & \frac{\Delta y}{\Delta x}+\frac{\Delta x}{\Delta y} \\ 4\frac{\Delta y}{\Delta x}-2\frac{\Delta x}{\Delta y} & -8\left(\frac{\Delta y}{\Delta x}+\frac{\Delta x}{\Delta y}\right) & 4\frac{\Delta y}{\Delta x}-2\frac{\Delta x}{\Delta y} \\ \frac{\Delta y}{\Delta x}+\frac{\Delta x}{\Delta y} & 4\frac{\Delta x}{\Delta y}-2\frac{\Delta y}{\Delta x} & \frac{\Delta y}{\Delta x}+\frac{\Delta x}{\Delta y} \end{bmatrix} T \tag{A27}$$

where the two-dimensional version of the stability parameter [38] is

$$\tau = \beta\left(\frac{u\Delta x + v\Delta y}{u^2+v^2}\right) \tag{A28}$$

for large $\mathbf{P}_e$. The β coefficient can be chosen to optimize the method with respect to its dispersive characteristics. The components of the skew-symmetric portions of the advective operator are given by the fourth and fifth terms, while the symmetric portion is the sixth term, which can also be written as

$$-\frac{1}{6}\left(u^2\frac{\Delta y}{\Delta x}\begin{bmatrix} 1 & -2 & 1 \\ 4 & -8 & 4 \\ 1 & -2 & 1 \end{bmatrix} + 3uv\begin{bmatrix} -1 & 0 & 1 \\ 0 & 0 & 0 \\ 1 & 0 & -1 \end{bmatrix} + v^2\frac{\Delta x}{\Delta y}\begin{bmatrix} 1 & 4 & 1 \\ -2 & -8 & -2 \\ 1 & 4 & 1 \end{bmatrix}\right)$$

showing that the symmetric portion of the advective operator induced by SUPG contains a cross term and therefore cannot be resolved into x- and y-components as in the finite volume methods.

A.10. Control volume finite element method (CVFEM)

The stencil for the CVFEM reads:

$$\frac{\Delta x\Delta y}{64}\begin{bmatrix} 1 & 6 & 1 \\ 6 & 36 & 6 \\ 1 & 6 & 1 \end{bmatrix}\dot{T} + \frac{u\Delta y}{16}\begin{bmatrix} -1 & 0 & 1 \\ -6 & 0 & 6 \\ -1 & 0 & 1 \end{bmatrix} T + \frac{v\Delta x}{16}\begin{bmatrix} 1 & 6 & 1 \\ 0 & 0 & 0 \\ -1 & -6 & -1 \end{bmatrix} T$$

$$= \frac{\alpha}{8}\begin{bmatrix} \frac{\Delta y}{\Delta x}+\frac{\Delta x}{\Delta y} & 6\frac{\Delta x}{\Delta y}-2\frac{\Delta y}{\Delta x} & \frac{\Delta y}{\Delta x}+\frac{\Delta x}{\Delta y} \\ 6\frac{\Delta y}{\Delta x}-2\frac{\Delta x}{\Delta y} & -12\left(\frac{\Delta y}{\Delta x}+\frac{\Delta x}{\Delta y}\right) & 6\frac{\Delta y}{\Delta x}-2\frac{\Delta x}{\Delta y} \\ \frac{\Delta y}{\Delta x}+\frac{\Delta x}{\Delta y} & 6\frac{\Delta x}{\Delta y}-2\frac{\Delta y}{\Delta x} & \frac{\Delta y}{\Delta x}+\frac{\Delta x}{\Delta y} \end{bmatrix} T \tag{A29}$$

The advective operator contains only skew-symmetric components, given by the second and third terms in the equation.

A.11 Control-volume finite element method with SUCV (CVFEM-SUCV)

The SUCV method results in a scheme similar to SUPG:

$$\frac{\Delta x\Delta y}{64}\begin{bmatrix}1&6&1\\6&36&6\\1&6&1\end{bmatrix}\dot{T}+\tau\frac{u\Delta y}{16}\begin{bmatrix}1&0&-1\\6&0&-6\\1&0&-1\end{bmatrix}\dot{T}+\tau\frac{v\Delta x}{16}\begin{bmatrix}-1&-6&-1\\0&0&0\\1&6&1\end{bmatrix}\dot{T}$$

$$+\frac{u\Delta y}{16}\begin{bmatrix}-1&0&1\\-6&0&6\\-1&0&1\end{bmatrix}T+\frac{v\Delta x}{16}\begin{bmatrix}1&6&1\\0&0&0\\-1&-6&-1\end{bmatrix}T$$

$$-\frac{\tau}{8}\begin{bmatrix}u^2\frac{\Delta y}{\Delta x}-4uv+v^2\frac{\Delta x}{\Delta y} & 6v^2\frac{\Delta x}{\Delta y}-2u^2\frac{\Delta y}{\Delta x} & u^2\frac{\Delta y}{\Delta x}+4uv+v^2\frac{\Delta x}{\Delta y}\\ 6u^2\frac{\Delta y}{\Delta x}-2v^2\frac{\Delta x}{\Delta y} & -12\left(u^2\frac{\Delta y}{\Delta x}+v^2\frac{\Delta x}{\Delta y}\right) & 6u^2\frac{\Delta y}{\Delta x}-2v^2\frac{\Delta x}{\Delta y}\\ u^2\frac{\Delta y}{\Delta x}+4uv+v^2\frac{\Delta x}{\Delta y} & 6v^2\frac{\Delta x}{\Delta y}-2u^2\frac{\Delta y}{\Delta x} & u^2\frac{\Delta y}{\Delta x}-4uv+v^2\frac{\Delta x}{\Delta y}\end{bmatrix}T$$

$$=\frac{\alpha}{8}\begin{bmatrix}\frac{\Delta y}{\Delta x}+\frac{\Delta x}{\Delta y} & 6\frac{\Delta x}{\Delta y}-2\frac{\Delta y}{\Delta x} & \frac{\Delta y}{\Delta x}+\frac{\Delta x}{\Delta y}\\ 6\frac{\Delta y}{\Delta x}-2\frac{\Delta x}{\Delta y} & -12\left(\frac{\Delta y}{\Delta x}+\frac{\Delta x}{\Delta y}\right) & 6\frac{\Delta y}{\Delta x}-2\frac{\Delta x}{\Delta y}\\ \frac{\Delta y}{\Delta x}+\frac{\Delta x}{\Delta y} & 6\frac{\Delta x}{\Delta y}-2\frac{\Delta y}{\Delta x} & \frac{\Delta y}{\Delta x}+\frac{\Delta x}{\Delta y}\end{bmatrix}T \tag{A30}$$

The skew-symmetric part of the advective operator remains the same as in CVFEM, while the symmetric portion, giving rise to artificial diffusion, is given by the 6th term in the foregoing formula. Similar to FEM, this term can be separated into three pieces, except the 4-8-4 columns and rows of SUPG become 6-12-6, (with the same signs) in the SUCV.

ACKNOWLEDGEMENTS

The authors would like to acknowledge Tim Trucano and Tom Smith for their helpful comments during the preparation of this report. This work was supported under the ASCI Advanced Spatial Discretization project. Sandia is a multiprogram laboratory operated by Sandia Corporation, a Lockhead Martin Company for the United States Department of Energy's National Nuclear Security Administration under contract DE-AC04-94AL8500.

REFERENCES

1. Fromm JE. A method for reducing dispersion in convective difference schemes. *Journal of Computational Physics* 1968; **3**:170–189.
2. Swaminathan CR, Voller VR. Streamline upwind scheme for control-volume finite elements, part 1. Formulations. *Numerical Heat Transfer, Part B* 1992; **22**:95–107.
3. Swaminathan CR, Voller VR. Streamline upwind scheme for control-volume finite elements, part 2. Implementation and comparison with the supg finite-element scheme. *Numerical Heat Transfer*, *Part B* 1992; **22**:109–124.
4. Vichnevetsky R, Bowles JB. *Fourier Analysis of Numerical Approximations of Hyperbolic Equations*. SIAM: Philadelphia, PA, 1982.
5. Robert Vichnevetsky. Wave propagation and reflection in irregular grid for hyperbolic equations. *Technical Report* MAE-1713, Department of Mechanical and Aerospace Engineering, Princeton University, July 1985.
6. Vichnevetsky R. Wave propagation analysis of difference schemes for hyperbolic equations: a review. *International Journal for Numerical Methods in Fluids* 1987; **7**:409–452.
7. Baptista AM, Adams EE, Gresho P. Benchmarks for the transport equation: the convection-diffusion equation and beyond. *Quantitative Skill Assessment for Coastal Ocean Models* 1995; **47**:241–268.
8. Gresho PM, Sani RL. *Incompressible Flow and the Finite Element Method*, *Advection-Diffusion and Isothermal Laminar Flow*. Wiley: Chicester, England, 1998.
9. Jansen KE, Collis SC, Whiting C, Shakib F. A better consistency for low-order stabilized finite element methods. *Computer Methods in Applied Mechanics and Engineering* 1999; **174**:153–170.
10. Ted Belytschko and Robert Mullen. On dispersive properties of finite element solutions. In *Modern Problems in Elastic Wave Propagation*, *International Union of Theoretical and Applied Mechanics*, Milóvitz J, Achenbach JD (eds). Wiley: New York, 1978; 67–82.
11. Vichnevetsky R, Tomalesky AW. Spurious wave phenomena in numerical approximations of hyperbolic equations. In *Proceedings of the Fifth Annual Princeton Conference on Information Science and Systems*, Princeton University, March 1971; 357–363.
12. Vichnevetsky R, De Schutter F. A frequency analysis of finite difference and finite element methods for initial value problems. In *AICA International Symposium on Computer Methods for Partial Differential Equations*, Lehigh University, Bethlehem, Pennsylvania, June 1975; 179–185.
13. Vichnevetsky R, Pariser EC. High order numerical sommerfeld boundary conditions: theory and experiments. *Computers and Mathematics with Applications* 1985; **11**(1–3):67–78.
14. Vichnevetsky R. On wave propagation in almost periodic structures. *Applied Numerical Mathematics* 1992; **10**:195–229.
15. Trefethen LN. Group velocity in finite difference schemes. *SIAM Review* 1982; **24**(2):113–136.
16. Karni S. On the group velocity of symmetric and upwind numerical schemes. *International Journal for Numerical Methods in Fluids* 1994; **18**:1073–1081.
17. Park KC, Flaggs DL. A Fourier analysis of spurious mechanisms and locking in the finite element method. *Computer Methods in Applied Mechanics and Engineering* 1984; **46**:65–81.
18. Park KC, Flaggs DL. A symbolic Fourier synthesis of a one-point integrated quadrilateral plate element. *Computer Methods in Applied Mechanics and Engineering* 1985; **48**:203–236.
19. Alvin KF, Park KC. Frequency-window tailoring of finite element models for vibration and acoustics analysis. In *Structural Acoustics*, *AMD*-vol. 128. ASME: New York, 1991; 117–128.
20. Shakib F, Hughes TJR. A new finite element formulation for computational fluid dynamics: Ix, Fourier analysis of space-time Galerkin/least-squares algorithms. *Computer Methods in Applied Mechanics and Engineering* 1991; **87**:35–58.
21. Harari I, Hughes TJR. Galerkin/Least-Squares finite element methods for the reduced wave equation with non-reflecting boundary conditions in unbounded domains. *Computer Methods in Applied Mechanics and Engineering* 1992; **98**:411–454.
22. Deville MO, Mund EH. Fourier analysis of finite element preconditioned collocation schemes. *SIAM Journal for Scientific and Statistical Computing* 1992; **13**(2):596–610.

23. Thompson LL, Pinsky PM. Complex wavenumber Fourier analysis of the p-version finite element method. *Computational Mechanics* 1994; **13**:255–275.
24. Grosh K, Pinsky PM. Complex wave-number dispersion analysis of Galerkin and Galerkin least-squares methods for fluid-loaded plates. *Computer Methods in Applied Mechanics and Engineering* 1994; **113**:67–98.
25. Nance DV, Viswanathan K, Sankar LN. Low-dispersion finite volume scheme for aeroacoustic applications. *AIAA Journal* 1997; **35**(2):255–262.
26. Christon MA. The influence of the mass matrix on the dispersive nature of the semi-discrete, second-order wave equation. *Computer Methods in Applied Mechanics and Engineering* 1999; **173**:147–166.
27. Voth TE, Christon MA. Discretization errors associated with reproducing kernel methods: one-dimensional domains. *Computer Methods in Applied Mechanics and Engineering* 2001; **190**:2429–2446.
28. Christon MA, Voth TE. Results of von Neumann analyses for reproducing kernel semi-discretizations. *International Journal for Numerical Methods in Engineering* 2000; **47**:1285–1301 (Invited paper from the Fourth World Congress on Computational Mechanics).
29. Mullen R, Belytschko T. Dispersion analysis of finite element semi-discretizations of the two-dimensional wave equation. *International Journal for Numerical Methods in Engineering* 1982; **18**:1–29.
30. Christon MA, Voth TE, Martinez MJ. Generalized fourier analysis of semi-discretizations of the advection–diffusion equation. *Technical Report SAND*2002-3866, Sandia National Laboratory, Albuquerque, New Mexico, November 2002.
31. van Leer B. Towards the ultimate conservative difference scheme. v. a second-order sequel to godunov's method. *Journal of Computational Physics* 1979; **32**:101–136.
32. Anderson WK, Bonhaus DL. An implicit upwind algorithm for computing turbulent flows on unstructured grids. *Computers and Fluids* 1994; **23**:1–21.
33. Leonard BP. A stable and accurate convective modelling procedure based on quadratic upstream interpolation. *Computer Methods in Applied Mechanics and Engineering* 1979; **19**:59–98.
34. Leonard BP. Simple high-accuracy resolution program for convective modelling of discontinuities. *International Journal for Numerical Methods in Fluids* 1988; **8**:1291–1318.
35. Leonard BP. Comparison of truncation error of finite-difference and finite-volume formulations of convective terms. *Applied Mathematical Modelling* 1994; **18**:46–50.
36. Gresho PM, Chan ST, Lee RL, Upson CD. A modified finite element method for solving the time-dependent, incompressible Navier–Stokes equations. Part 1: theory. *International Journal for Numerical Methods in Fluids* 1984; **4**:557–598.
37. Raymond WH, Gardner A. Selective damping in a Galerkin method for solving wave problems with variable grids. *Monthly Weather Review* 1976; **104**:1583–1590.
38. Brooks AN, Hughes TJR. Streamline upwind/Petrov–Galerkin formulations for convection dominated flows with particular emphasis on the incompressible Navier–Stokes equations. *Computer Methods in Applied Mechanics and Engineering* 1982; **32**:199–259.
39. Tezduyar TE. *Stabilized Finite Element Formulations for Incompressible Flow Computations*, vol. 28. Academic Press, Inc.: San Diego, CA, 1992; 1–44.
40. Lee RL, Gresho PM, Chan ST, Sani RL, Cullen MJP. *Finite Elements in Fluids*, vol. 4. Chapter Conservation laws for primitive variable formulations of the incompressible flow equations using the Galerkin finite element method. Wiley: Chichester, England, 1982; 21.